Saudi Pharmaceutical Journal 31 (2023) 1061–1076

HOSTED BY

Contents lists available at ScienceDirect

Saudi Pharmaceutical Journal

journal homepage: www.sciencedirect.com

Original article

Tanshinone-I for the treatment of uterine fibroids: Molecular docking, simulation, and density functional theory investigations

Abhishek Tiwari [a,*], Varsha Tiwari [a], Ajay Sharma [b], Deependra Singh [c], Manju Singh Rawat [c], Tarun Virmani [d], Reshu Virmani [d], Girish Kumar [d], Manish Kumar [e], Abdulsalam Alhalmi [f], Omar M. Noman [g], Ramzi A. Mothana [g], Mohammad Alali [h]

[a] Department of Pharmacy, Pharmacy Academy, IFTM University, Lodhipur-Rajpur, Moradabad 244102, India
[b] Delhi Pharmaceutical Sciences and Research University, Pushp Vihar, New Delhi 110017, India
[c] University Institute of Pharmacy, Pt. Ravi Shankar Shukla University, Raipur, Chhattisgarh, India
[d] School of Pharmaceutical Sciences, MVN University, Palwal, Haryana 121105, India
[e] School of Pharmaceutical Sciences, CT University, Ludhiana- 142024 Punjab, India
[f] Department of Pharmaceutical Sciences, College of Pharmacy, Aden University, Aden, Yemen
[g] Department of Pharmacognosy, College of Pharmacy, King Saud University, Riyadh 11451, Saudi Arabia
[h] Institute of Pharmacy, Clinical Pharmacy, University of Greifswald, Friedrich-Ludwig-Jahn-Str. 17, 17489 Greifswald, Germany

ARTICLE INFO

Article history:
Received 14 February 2023
Accepted 1 May 2023
Available online 8 May 2023

Keywords:
Uterine fibroids
Molecular modelling
Tanshinone-I
Progesterone blocker
Docking

ABSTRACT

Uterine fibroids (UF), most prevalent gynecological disorder, require surgery when symptomatic. It is estimated that between 25 and 35 percent of women wait until the symptoms have worsened like extended heavy menstrual bleeding and severe pelvic pain. These UF may be reduced in size through various methods such as medical or surgical intervention. Progesterone (prog) is a crucial hormone that restores the endometrium and controls uterine function. In the current study, 28 plant-based molecules are identified from previous literature and docked onto the prog receptors with 1E3K and 2OVH. Tanshinone-I has shown the best docking score against both proteins. The synthetic prog inhibitor Norethindrone Acetate is used as a standard to evaluate the docking outcomes. The best compound, tanshinone-I, was analyzed using molecular modeling and DFT. The RMSD for the 1E3K protein–ligand complex ranged from 0.10 to 0.42 Å, with an average of 0.21 Å and a standard deviation (SD) of 0.06, while the RMSD for the 2OVH protein–ligand complex ranged from 0.08 to 0.42 Å, with an average of 0.20 Å and a SD of 0.06 showing stable interaction. In principal component analysis, the observed eigen values of HPR-Tanshinone-I fluctuate between −1.11 to 1.48 and −1.07 to 1.25 for PC1 and PC2, respectively (1E3K), and the prog-tanshinone-I complex shows eigen values of −38.88 to −31.32 and −31.32 to 35.87 for PC1 and PC2, respectively (2OVH), which shows Tanshinone-I forms a stable protein–ligand complex with 1E3K in comparison to 2OVH. The Free Energy Landscape (FEL) analysis shows the Gibbs free energy in the range of 0 to 8 kJ/mol for Tanshinone-I with 1E3K and 0 to 14 kJ/mol for Tanshinone-I with the 2OVH complex. The DFT calculation reveals ΔE value of 2.8070 eV shows tanshinone-I as a stable compound. 1E3K modulates the prog pathway, it may have either an agonistic or antagonistic effect on hPRs. Tanshinone-I can cause ROS, apoptosis, autophagy (p62 accumulation), up-regulation of inositol requiring protein-1, enhancer-binding protein homologous protein, p-c-Jun N-terminal kinase (p-JNK), and suppression of MMPs. Bcl-2 expression can change LC3I to LC3II and cause apoptosis through Beclin-1 expression.

* Corresponding author.
E-mail addresses: abhishekt1983@gmail.com (A. Tiwari), varshat1983@gmail.com (V. Tiwari), ajaysharmapharma1979@gmail.com (A. Sharma), deependraiop@gmail.com (D. Singh), manjursu@gmail.com (M. Singh Rawat), tarun.virmani@mvn.edu.in (T. Virmani), reshu.virmani@mvn.edu.in (R. Virmani), girish.kumar@mvn.edu.in (G. Kumar), manish_singh17@rediffmail.com (M. Kumar), onoman@ksu.edu.sa (O.M. Noman), rmothana@ksu.edu.sa (R.A. Mothana), S-moalal@uni-greifswald.de (M. Alali).

Peer review under responsibility of King Saud University. Production and hosting by Elsevier.

Production and hosting by Elsevier

https://doi.org/10.1016/j.jsps.2023.05.002
1319-0164/

1. Introduction

Tumors of the uterine lining, sometimes called leiomyomas (UFs), are frequent benign gynecological tumors that develop from the proliferation of smooth muscle cells in the uterus (Fig. 1A) (Okesola et al., 2022). It's estimated that 70–80% of women will be affected by them at some point in their lives and vast majority of those cases will show no symptoms at all (Don et al., 2022). Abnormal bleeding, pelvic discomfort, menorrhagia, infertility, miscarriages, and other obstetric difficulties are all clinical indications of UF that contribute to poor quality of life (Keizer et al., 2022; Piriyev and Römer, 2023; Yudha Pratama Putra et al., 2021).

Although the precise origin of UF is unknown, several variables have been linked to its pathogenesis, including genetics, cytokines, growth factors, hormones including estrogen and prog and/or their receptors, the environment, epigenetics, and the overproduction of extracellular matrix (ECM) (Al-Hendy et al., 2021; Czarnik et al., 2023).

There are several therapies that may be employed, i.e., pharmacological, surgical, and radiological techniques, including uterine embolization or magnetic resonance targeted ultrasound. Hysterectomy, meanwhile, continues to be the standard, one-size-fits-all approach for fibroids. Nevertheless, numerous women require a successful substitute to a hysterectomy due to numerous reasons, namely quicker healing and the preservation of reproductive ability. As a result, conservative solutions are required, and secure and efficient pharmacological intervention is one of them.

Tranexamic acid, oral contraceptives, oral and injectable prog, Prog-releasing intrauterine systems, antiprogesterone, gonadotropin-releasing hormone (GnRH) agonists and antagonists, selective prog receptor modulators (SPRMs), selective oestrogen receptor modulators (SERMs), aromatase inhibitors, danazol, and gestrinone are some of the medical interventions currently available. The majority of these treatments do not particularly target UF; rather, they are employed to regulate irregular UF. Prog. is among those employed most frequently.

Prog is a vital hormone, regulates uterine function, principally involved in the restoration of the endometrium. Prog interaction with the human prog receptor (HPR), comes under the nuclear hormone receptor superfamily, represents the joint functions of PR-A and B. Upon ligand binding, these may affect cellular physiology and alter gene expression through two methods: (i) PRs act as ligand-activated transcription factors to directly interact with DNA promoter transcription and modulate the downstream genes expression (ii) PRs interact through Src tyrosine kinases and trigger MAPKs, which affect gene functioning (Boonyaratanakornkit et al., 2001; Boonyaratanakornkit and Edwards, 2007; Leonhardt et al., 2003; Patel et al., 2015).

It has been shown that Prog promotes UFs growth by increasing the number of cells, size as well as ECF amount. Proteins called PR-A and PR-B were also found to be higher in fibroids than in healthy myometrium. Both Prog and growth factor are linked to several processes, such as cell growth and death (apoptosis) (Fig. 1). Therefore, Prog blockers may play an effective role in the treatment of UFs. Phyto-constituents possess enormous potential in the management of life threatening diseases. Many phytoconstituents e.g., curcumin, quercetin, rutin etc are reported to possess anticancer potential.

Therefore, the present study has been designed to explore the potential of 28 phytochemicals from different plants to block the human prog receptor as a therapy for uterine fibroids using in-silico methods. Fig. 2 shows the schematic illustration of the present study for the discovery of potential prog receptor inhibitors.

CAM therapy may turn out to be a good way to treat UF. Literature shows that Gui Zhi Fu Ling Tang, *Ramulus cinnomomi*, and *Poriae cocos* decoction, *Danshen Gegen* decoction (*Salviae Miltiorrhizae* Radix, *Purariae Lobatae*, Radix decoction), Genistein, Green Tea (*Camellia sinensis*), and Tanshinone-I are effective against UF.

Tanshinone-I is obtained from *Salviae miltiorrhizae* and employed in the treatment of atherosclerosis, downregulation of adhesion molecules, and enhancement of microcirculation by stimulating endothelium-dependent vasodilatation (EDVD) in coronary arterioles through the neuromodulators endothelial nitric oxide synthase (eNOS) and angiotensin II. Interestingly, it also stops the growth of vascular smooth muscle cells (VSM) and thins the intima. It does this by cleaving caspase-3 to promote cell death and blocking the PI3K/AKT/mTOR pathway to cause autophagy (Ansari et al., 2021; Dalton-Brewer, 2016).

2. Materials and methods

2.1. Molecular docking study

The molecular docking studies of the identified compounds were performed on a 5950 X 16-Core Processor (3.40 GHz); AMD Ryzen-9; Windows 10 (64-bit); and 64-GB RAM.

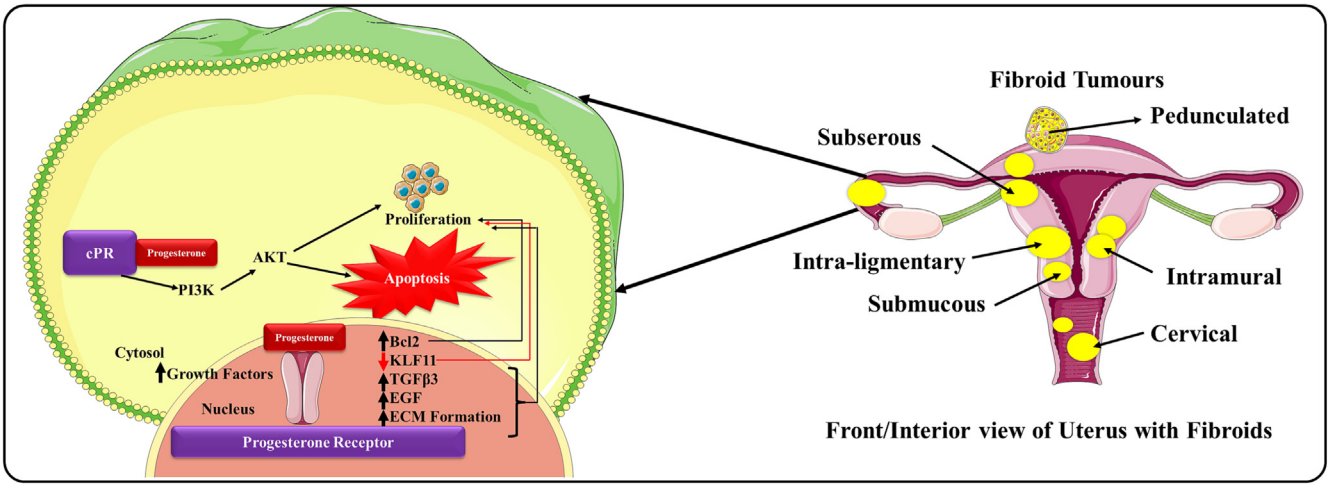

Fig. 1. Interrelation of Prog and growth factors in fibroid management.

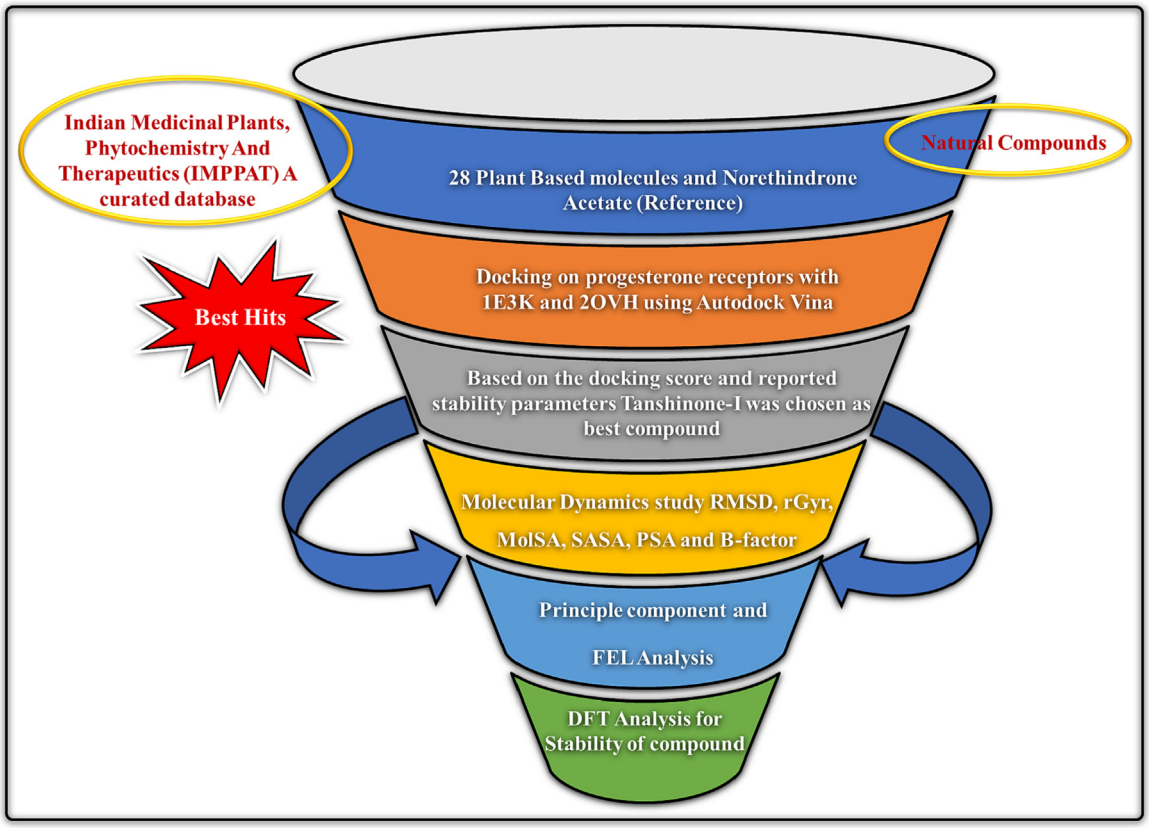

Fig. 2. Schematic illustration of the present study for the discovery of potentialprog receptor inhibitors.

2.2. Selection and protein receptors from PDB:

We have collected all reported structures from PDB (https://www.rcsb.org) and compared them to one another in order to explore the variability in the ligand binding patterns in different crystal structures of human PR. Their receptors were thoroughly examined as well. In order to examine SPRMs and human PRs, we have selected two PDBs i.e., 1E3K and 2OVH from the RCSB database. Protein preparation was carried out using the Autodock Wizard by deleting attached water molecules, bound heteroatoms or ligands, adding polar hydrogens, Kollman charges, spreading charge equally over all atoms, and checking for missing atoms on residues. The PDB files were then converted to the PDBQT format for executing the next step. Table 1 shows the details of all human prog receptor structures retrieved from the PDB 2 database (Saritha et al., 2023).

Table 1
Human prog receptors from PDB 2 database.

Category	PDB	Ligand	Resolution (A^0)
GROUP-1	2W8Y	Mifepristone (MT)	1.8
Steroidal antagonist	4A2J	Asoprisnil (AS)	2.0
	4OAR	Ulipristal acetate (UA)	2.41
	2OVH	Asoprisnil	2.0
	2OVM	Asoprisnil	2.6
GROUP-2	4APU	A2K	1.9
(Non-steroidal SPRM)	3G8O	30X	1.90
	3ZR7	OR8	1.65
	3HQ5	GKK	2.1
	3KBA	WOW	2.0
GROUP-2	1A28	PROGESTERONE (STR)	1.8
Steroidal Agonist	1E3K	Metribolone (R18)	2.8
	1SR7	Mometasone furoate	1.46
	3D9O	Levonorgestrel	2.26
GROUP-2	1ZUC	Tanaproget (T98)	2.0
Non-steroidal Agonist			

2.3. Molecular docking procedure

2.3.1. Grid generation

For carrying out docking between prepared receptors and ligands, grid was generated by taking the center on the attached ligand. The grid dimensions are given in Table 2.

Table 2
Grid Parameters.

S. No.	Parameters	1E3K	2OVH
1)	**Exhaustiveness**	8	8
2)	**center_x**	28.6348	30.6727
3)	**center_y**	−7.7984	0.7615
4)	**center_z**	9.5311	28.3292
5)	**size_x**	16.0747	16.0146
6)	**size_y**	16.1977	16.1716
7)	**size_z**	16.1712	16.1487

2.3.2. For PDB 1E3K

The crystallographic 3D structure of the Human Prog Receptor (HPR) Ligand Binding Domain in complex with the ligand metribolone (R1881) was accessed from Protein Data Bank (PDB ID code 1E3K) with unit cell (Å) a = 58.402, b = 65.011, c = 71.181, and angles (°) α = 90, β = 95.65 and γ = 90 respectively. The resolution of the X-Ray Diffraction (XRD) structure of this model enzyme is 2.80 Å. After optimizing hydrogen bonds, OPLS-2005 was used as the force field to refine the structure minimization to an RMSD constraint value of 0.3 Å. Grid box dimensions were 16.0747 X 16.1977 X 16.1712 (all in Å) with a 0.375 Å grid point spacing.

Protein residues that include ligand-restricting sites are logically expected to contain certain ligands that can bind reversibly. The correct orientation for other protein-affirming amino acid residues was provided.

2.3.3. For PDB 2OVH

Protein Data Bank (PDB ID code 2OVH) provided access to the crystallographic 3D structure of the prog receptor with bound Asoprisnil and a peptide from the co-repressor SMRT, with unit cell (a) = 87.475, b = 87.475, c = 90.599, and angles (°) α = 90, β = 90, and γ = 120, respectively. This model enzyme's XRD structure has a resolution of 2.00 Å. After optimizing hydrogen bonds, the structural reduction was further refined using the OPLS-2005 force field to achieve the 0.20 Å RMSD constraint value. The grid box measures 16.0146 × 16.1716 × 16.1487 (all in Å) with a grid point spacing of 0.375 Å. It stands to reason that certain ligands with reversible binding capabilities would be present in protein residues with ligand-restricting sites. Other protein-affirming amino acid residues were given the proper orientation.

2.4. Selection and preparation of phytoconstituents

28 phytochemicals are selected on the basis of a review of the literature from search engines and the IMPPAT 2.0 database, which provides extensive information with 100 books and 7000 + research articles on Indian medicine. The phytoconstituents are selected on the basis of their antitumor effects. In order to virtually test the ability of phytoconstituents to bind to specific proteins, this database provides information regarding phytochemicals, medical applications, as well as 2D and 3D chemical structures. Table 3 shows the phytoconstituents selected for the study with their IMPPAT-ID (https://cb.imsc.res.in/imppat/). All the phytoconstituents were downloaded in SDF format from PubChem, their energy reduced by the MMFF94 Force Field, and then opened in the PyRx program, which converted them to PDBQT format. The LigPrep application (the trial version of Schrödinger) was used to prepare the ligands. Energy optimization for all ligands was done using the OPLS 2005 force field, but the 0.01 Å RMSD cut-off was not reached. At the desired pH of 7 ± 2, Epic was used to produce tautomers, all conceivable ionization states, and low energy ring conformations for each ligand. The output format of the Schrodinger Maestro was used to save the prepared ligands.

2.5. Docking and visualization of results

Docking was used to collect a set of ligand-binding site conformations and orientations. PyRx, AutoDock-Vina scoring-function-based analysis of binding sites, and docking runs of target proteins with ligands. Each ligand's conformations were analyzed, and the ones with the highest binding affinities were selected. Maestro Visualizer was used to generate the 3D and 2D interaction diagrams.

2.6. Molecular dynamics simulations

The Desmond tool from Schrödinger's suite was used to do molecular dynamics simulations on the ligand–protein combination (Bowers et al., 2006).The best chemical from those that passed screening was chosen for MD simulations using criteria including the number of hydrogen bonds, binding energy, and glide score. Tanshinone-I, the best docked chemical, was chosen for simulation analysis in this investigation. We neutralized the charge and adjusted the salt content to 0.15 M of Na^+ and Cl^- ions to create the physiological condition of the simulation box. Aligning the major axes of the solute along the box vectors or the diagonal reduces the volume of the simulation box. Proteins, protein complexes, protein–ligand complexes, proteins embedded in a membrane bilayer, etc. make up the solute in the solvated system. By doing a 100 ps low-temperature (100^0K) Brownian motion MD simulation (NVT ensemble), we were able to remove steric conflicts in the complex and reduce the energy of the ligand–protein interaction. From the MD tab's work space, we loaded the pre-processed ligand protein complex, and then we adjusted the temperature to 300^0 K and the pressure to 1.01325 bar in the NPT ensemble. The ligand–protein complex's trajectory was measured at 4.8 ps after 100 ns of simulations, which were run after the model system was relaxed. The conformational behaviour and stability of the complex were examined by calculating and analyzing energy, ligand–protein RMSD, RMSF, protein–ligand interactions, and ligand characteristics throughout the course of a 100 ns simulation.

2.7. Analysis of simulation data

After analyzing the MD trajectories, the root-mean-square deviation (RMSD), root-mean-square fluctuation (RMSF), and other measures for the distance between residues and inhibitors were computed using the VMD (version: 1.9.1) or in-house Perl scripts.

2.8. Principal component analysis (PCA)

The large-amplitude movements were analyzed with a principal component analysis (PCA). The eigenvalues and eigenvectors were analyzed with the covariance matrix that was constructed from the diagonalized covariance matrix. The principal components (PCs), also known as eigenvectors, reveal the motional orientation of the ligand and receptor atoms, while the corresponding eigenvalues characterize the mean square fluctuations of the complex. Using calculations and graphs, PC1 and PC2 were used to validate their motions (Dalal et al., 2021).

2.9. FEL analysis

The FEL along the PC was postulated in order to better understand the energy distribution of the protein folding route during molecular dynamics. The formula for calculating the free energy of a protein is (Eq. (1):

$$\Delta G = \Sigma - KTB\,ln\,(PA - PB) \quad (1)$$

-where △G represents the Gibbs energy landscape, TB is the gas constant, and K is the equilibrium constant. PA and PB represent the two protein probabilities along the dynamic pathway. Using the eigenvector values obtained from the PCA, 3D FEL plots of protein–ligand complexes were created. To analyze the maximum and minimum energy of drug complexes, a FEL plot with different contour maps of various color patterns, such as red, yellow, green, orange, and blue, was generated (Dalal et al., 2021).

2.10. Density functional theory (DFT) analysis

The phytochemical reactivity was analyzed with DFT. The analysis used the highest occupied molecular orbital (HOMO) and the lowest unoccupied molecular orbital (LUMO) energies. The expression was used to figure out the band energy gap. All of these labels come straight from the calculations of quantum physics. This formula was used to determine the HOMO–LUMO energy difference (Eq. (2):

$$\Delta E = E_{LUMO} - E_{HOMO} \quad (2)$$

The HOMO and LUMO energies to get the chemical potential (μ) (Eq. (3), chemical hardness (η) (Eq. (4) and chemical softness (σ) (Eq. (5) of the system:

Table 3
Phytochemicals isolated from fruits and vegetables for Fibroid treatment and their mechanisms of action.

S. No.	Name	IMPPAT ID	Biological sources	Uses	References
1.	Apigenin	IMPHY004661	*Lonicera gracilipes* var. *glandulosa*	Anticancer	(Si et al., 2009; Wu et al., 2005)
2.	Equol	IMPHY005820	*Pueraria mirifica* and *Cordyceps militaris*	Cancer	(Axelson et al., 1982; Setchell et al., 2005; Wang et al., 2014)
3.	Daidzein	IMPHY004566	*Pueraria mirifica* and *Cordyceps militaris*	Anti-oxidant, anti-carcinogenic	(E. Kim et al., 2015; Sakamoto et al., 2016)
4.	Genistein	IMPHY004643	*Flemingia vestita*	Anticancer	(Choi et al., 2020; Hwang et al., 2020; Liang et al., 2018)
5.	Catechin	IMPHY014854	*Camellia sinensis*	Anticancer	(Alshatwi, 2010; Cheruku et al., 2018; Waffo-Téguo et al., 2001)
6.	Myricetin	IMPHY005471	*Tibouchina paratropica*	Antimicrobial	(Jinwal et al., 2009; Phillips et al., 2011; Semwal et al., 2016; Tzeng et al., 1991; Xu et al., 2016)
7.	Isorhamnetin	IMPHY008724	*Pollen typhae*	Anti-cancer	(Hu et al., 2015; Kim et al., 2011)
8.	Fisetin	IMPHY005433	*Galeditsia triacanthos*	Antioxidant, Anticancer, Neuroprotection	(S. C. Kim et al., 2015; Mukhtar et al., 2015)
9.	Eriocitrin	IMPHY012252	Citrus limon	Anticancer	(Wang et al., 2016)
10.	Tanshinone-I	IMPHY010828	*Salvia miltiorrhiza*	Anticancer	(Su and Chiu, 2016; Xie et al., 2015; Zhang et al., 2016)
11.	Naringenin	IMPHY010550	*Aglaia duperreana*	Anticancer	(Saponara et al., 2006)
12.	Taxifoline	IMPHY011967	Silybum marianum	Anticancer	(Angelis et al., 2016; Ren et al., 2020)
13.	Myricetin	IMPHY005471	*Myrica nagi* Thunb.	Anti-oxidant, anticancer, antidiabetic and anti-inflammatory	(Du et al., 2012)
14.	(-) Gallocatechin	IMPHY011735	*Saxifraga cuneifolia, Quercus dentata*	Antioxidant, anti-obesity activity	(Waffo-Téguo et al., 2001)
15.	(−)-Epicatechin	IMPHY014854	*Camellia Sinensin*	Anticancer	(Nogueira et al., 2011; Shay et al., 2015; Wang et al., 2015)
16.	(−)-Epigallocatechin	IMPHY011735	*Camellia Sinensin*	Anticancer	(Chung and Vadgama, 2015; Lee and Tan, 2015; Waffo-Téguo et al., 2001)
17.	(−)-Epicatechin 3-gallate	IMPHY011874	*Camellia Sinensin*	Anticancer	(Takizawa et al., 2003; Wang et al., 2013)
18.	(−)-Epigallocatechin 3-gallate	IMPHY011671	*Camellia Sinensin*	Anticancer	(Chiou et al., 2012; Ignasimuthu et al., 2019; Kannen et al., 2013)
19.	Flavone	————————	*Apium graveolens, Petroselinum crispum, artichoke Cynara scolymus*	Anticancer, Antioxidant	(Kellis and Vickery, 1984)
20.	Dihydrodibenzoxepin	IMPHY006809	*Bauhinia variegate*	Anti-cancer	(Lee et al., 2010)
21.	Glicentin	MPHY015706	Monoclonal anti-glucagon	Stimulation of insulin secretion, inhibition of gastric acid secretion	(Raffort et al., 2017)
22.	Kaemferol	IMPHY004388	*Lotus ucrainicus*	Antitumor	(An and Kim, 2015; Luo et al., 2012, 2011; Shin et al., 2015)
23.	Quercentin	IMPHY004619	*Camellia sinensis*	Anti-oxidant Atherosclerosis	(Liu et al., 2020; Navarro-Núñez et al., 2010; Yang et al., 2015)
24.	Cyanidin	IMPHY008945	*Rhododendron cv.*	Anticancer	(Cheng et al., 2009; Kannan and Kolandaivel, 2018; Lee et al., 2013)
25.	Pelargonidin	IMPHY003437	*Philodendron*	Anticancer	(Khandelwal and Abraham, 2014)
26.	Norethindrone Acetate	IMPHY013743	Synthetic second-generation progestin	Heavy periods, Breast cancer	(Cheng and Wolfe, 1983; Muneyyirci-Delale and Karacan, 1998)
27.	Eriodictyol	IMPHY004038	*Eriodictyon californicum*	Anticancer	(Zhang et al., 2020)
28.	Quercitrin	IMPHY015054	Citus families, berries	Anticancer	(Vafadar et al., 2020)
29.	Gnetol	IMPHY000794	Genus gnetum	Anticancer (tyrosinase inhibitor)	(Ohguchi et al., 2003)

$$\boldsymbol{\mu} = \frac{\boldsymbol{E_{LUMO} - E_{HOMO}}}{2\boldsymbol{e}} \tag{3}$$

$$\eta = \frac{\boldsymbol{E_{LUMO} - E_{HOMO}}}{2} \tag{4}$$

$$\sigma = \frac{1}{\eta} \tag{5}$$

The electron affinity (A) is equal to the LUMO energy level, while the ionization potential (I) is defined as the − E_{HOMO} energy level. The following equations can be used to determine the electronegativity (χ) (Eq. (6), electrophilicity (ω) (Eq. (7), maximum charge transfer (Eq. (8), and nucleophilia (Eq. (9) of a substance:

$$\chi = \frac{\mathbf{I} + \mathbf{A}}{2} \tag{6}$$

$$\omega = \frac{\boldsymbol{\mu}^2}{2\eta} \tag{7}$$

$$\Delta \mathbf{N_{max}} = \frac{\chi}{\eta} \tag{8}$$

$$(\mathbf{N}) = \boldsymbol{E_{LUMO} - E_{HOMO(TCE)}} \tag{9}$$

Table 4
Molecular Docking Results.

S. No.	Binding Affinity (kcal/mol)		Compound Name
	1E3K	2OVH	
1.	−9.2	−8.8	Apigenin
2.	−9.4	−8.9	Equol
3.	−9.5	−8.9	Daidzein
4.	−8.9	−9	Genistein
5.	−8.5	−8.5	Catechin
6.	−8.3	−8.7	Myricetin
7.	−8.3	−8.8	Isorhamnetin
8.	−9.3	−8.5	Fisetin
9.	−10.2	−9.9	Tanshinone-I
10.	−9	−8.7	Naringenin
11.	−8.9	−9	Eriodictyol
12.	−8.8	−8.8	Taxifoline
13.	−8.3	−8.9	Quercitrin
14.	−8.3	−8.7	Myricetol
15.	−8	−8.4	(+)-Gallocatechin
16.	−8.5	−8.5	(−)-Epicatechin
17.	−8	−8.4	(−)-Epigallocatechin
18.	−4.3	−9.5	(−)-Epicatechin 3-gallate
19.	−3.7	−9.2	(−)-Epigallocatechin 3-gallate
20.	−9	−8.6	Flavanone
21.	−8.1	−7.6	Dihydrodibenzoxepin
22.	−9	−8.8	Glycitein
23.	−8.8	−8.6	Kaemferol
24.	−8.3	−8.9	Quercetin
25.	−8.7	−8.6	Cyanidin
26.	−8.5	−8.4	Pelargonidin
27.	−8.1	−7.6	Gnetol
28.	−8.5	−7.8	Pterostilbene
29.	−10.7	−10.1	Norethindrone Acetate

3. Results

3.1. Docking results

The docking results are shown in Table 4. The docking interaction of 1E3K showed Tanshinone-I is the best docked compound when compared with the standard drug, as shown in Figs. 3 and 4. Other compounds like Equol, Fisetin, Genistein, Myrecetin, and Apigenin have showed good results and illustrated in the supplementary file Fig. 1a–5a. Table 5 shows the interacting amino acids with 1E3K, whereas Table 6 shows the interacting amino acids with the 2OVH receptor protein. The docking interaction of 2OVH showed Tanshinone-I is the best docked compound when compared with the standard drug, as shown in Figs. 5 and 6. Other compounds like (-)-Epicatechin 3-gallate, (-)-Epigallocatechin 3-gallate, Eriodictyol, Genistein, and Quercetin have shown good results and are shown in the supplementary file Fig. 6a–10a. Fig. 10a. 3d&2d- Docking interaction on 2OVH with Genistein has been showed below (Tiwari et al., 2022).

3.2. Prediction of ADMET analysis

The Swiss ADME software (https://www.swissme.ch) was used to estimate each ADME analysis (physicochemical properties, water solubility, lipophilicity, pharmacokinetics, and drug similarity). The results of the physicochemical properties of some phytochemicals are shown in supplementary table 1a. The results of lipophilicity, water solubility, pharmacokinetics, and drug-likeness are shown in supplementary tables 2a, 3a, 4a, and 5a, respectively, and included in the supplementary files. The lipophilic properties were put into three main groups: fragmental (based on fragments, wLog P), topological (based on descriptors, mLog P), and 3D physics-based (iLog P and xLog P, based on solvent free energy in octanol). The pink area represents the optimal range for each property (lipophilicity: MLOGP less than 4.15, XLOGP between −0.7 and + 5.0, size: MW between 150 and 500 g/mol, polarity: TPSA between 20 and 130 Å2, solubility: log S not higher than 6, saturation: the fraction of carbons in the sp3 hybridization not less than 0.25, and flexibility: no more than 9 rotatable bonds). From these results, the compound can be predicted not to be orally bioavailable, but to be too flexible and polar. Figs. 7-9 depict the protein–ligand RMSD, RMSF, and secondary structure of proteins, Ligand RMSF, and Protein Ligand Contacts for 1E3K and Figs. 10–12 for 2OVH, respectively. Results of (a) principal component analysis (b) FEL 3D, are shown in Fig. 13 for 1E3K and Fig. 14 for 2OVH. Fig. 15 depicts the HUMO and LUMO analyses of Tanshinone-I.

Results of Principle compnent analysis and FEL 3D for IE3K

3.3. Results from DFT analysis

The energy gap ΔE (eV) between EHOMO (eV) and ELUMO (eV) and other parameters are shown in Table 7.

4. Discussion

The development of synthetic prog ligands with either prog receptor (PR) agonist (progestins) or mixed agonist/antagonist action has been stimulated by the apparent, if uncertain, contribution of prog lead to the formation of fibroids. It has been

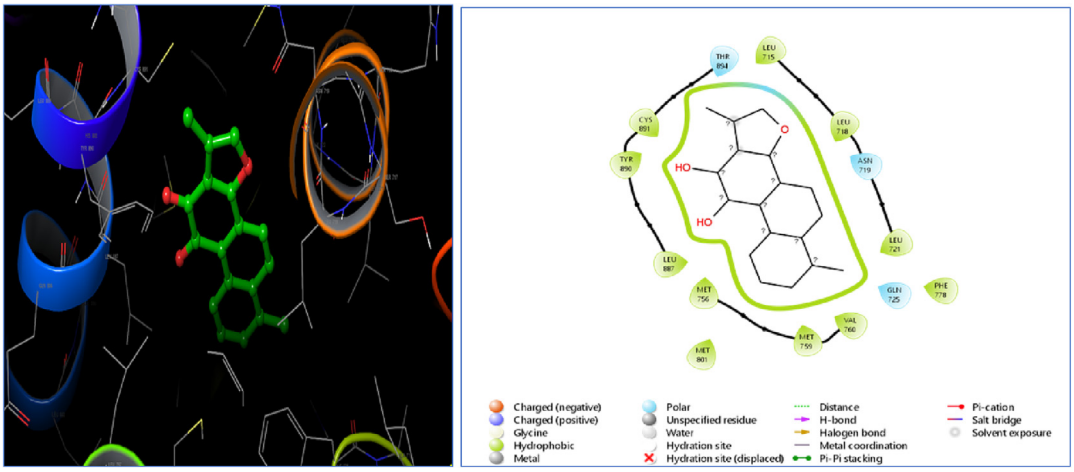

Fig. 3. 3d-&2d Docking interaction on 1E3K with Tanshinone-I.

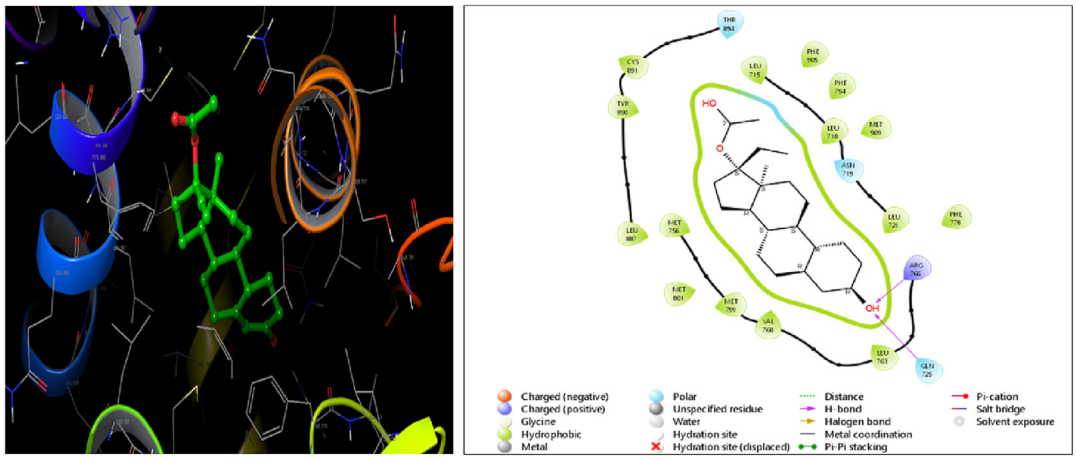

Fig. 4. 3d&2d- Docking interaction on 1E3K with Norethindrone Acetate.

demonstrated that prog and PR complexes decrease apoptosis and encourage fibroid cell growth. hPR-A and hPR-B are the two main isoforms of PRs. By means of two distinct promoters, the same gene can produce both isoforms. Another PR isoform, PR-M, is assumed to contribute to cellular respiration and provide shielding from apoptosis. It has nongenomic action. Recently, it was discovered that the fibroid edge has higher levels of PR-M expression and mitochondrial density than the myometrium. Thus, a non-genomic progestin-induced rise in cellular respiration may play a significant role in the development of fibroid.

Norethindrone acetate is used for menorrhagia associated with fibroids at a dose of 5–15 mg/day, which has been taken as the standard drug for the study. This belongs to the class of progestins and works by stopping the uterine lining from growing and stopping proliferation. This drug is associated with numerous side effects, namely irregular vaginal bleeding or spotting, menstrual flow modifications, enlarged/tender breasts, nausea, blood clots, vomiting, difficulty falling asleep, acne, brown patches on the face, hair loss and growth of hair on the face, etc. It works at the molecular level. Progestins like norethisterone affect target cells by binding to prog receptors, which change target genes. The reproductive system, the breast, the pituitary gland, the hypothalamus, the skeleton, and the central nervous system all have cells that are targets. Norethisterone also causes the endometrium to change in ways that make it unsuitable for implantation, such as shrinking, irregular secretion, and slowed growth. Tanshinone-I, which comes from plants, can be used instead of a synthetic standard drug.

The molecular docking studies revealed the promising potential of Tanshinone-I among the 28 docked compounds. The binding affinity of Tanshinone-I on 1E3K and 2OVH was found to be −10.2 and −9.9, respectively, which is comparable with that of standard Norethindrone Acetate on 1E3K and 2OVH, which is −10.7 and −10.1, respectively. Further, PCA and FEL data analysis of Tanshinone-I on the 1E3K receptor revealed a stable and strong interaction with the receptor, proving its promising role in the treatment of uterine fibroid.

Table 5
Hydrophobic and polar bond interaction of selected phytoconstituents with 1E3K Protein.

S. No.	Compound names	Hydrophobic bond	Polar bond
1.	Tanshinone-I	Val760; Met759; Met756; Met801; Leu887; Tyr890; Cys891; Leu715; Leu718; Leu721	Gln725; Asn719; Thr894
2.	Norethindrone Acetate	Leu763; Val760; Met759; Met756; Met801; Leu887; Tyr890; Cys891; Leu715; Phe905; Phe794; Leu718; Met909	Gln725; Asn719; Thr894
3.	Equol	Leu763; Met759; Phe794; Tyr890; Leu715; Leu718,	Asn719; Thr894; Thr716
4.	Fisetin	Phe778; Leu763; Val760; Met759; Met801; Met756; Leu887; Tyr890; Cys891; Val903; Leu715; Leu718; Leu721; Polar Charged Arg719, Gln725	Asn719; Thr894; Thr716
5.	Genistein	Leu763; Met801; Phe778; Met756; Met759; Leu887; Val760; Met759; Tyr890, Cys891, Met756; Leu715; Val903; Leu718; Leu721	Asn719; Thr894; Thr716
6.	Myrecetin	Leu763; Met801; Phe778; Met756; Met759; Leu887; Tyr890; Cys891; Met756; Leu715; Val903; Leu715; Leu718; Leu721	Asn719; Thr894; Thr716
7.	Apigenin	Leu763; Met759; Met756; Leu887; Tyr890; Cys891; Leu715; Leu718; Leu721; Tyr890	Asn719

Table 6
Hydrophobic and polar bond interaction of selected phytoconstituents with 2OVH Protein.

S. No.	Compound names	Hydrophobic bond	Polar bond
1	Epicatechin-3-gallate	Leu715; Leu718; Leu721; Leu726; Trp755; Met759; Val760; Leu763; Phe778; Leu 887; Tyr 890; Leu 797; Cys891	Asn719; Gln725
2	Eriodictyol	Leu721; Leu763; Phe778; Val760; Met759; Met756; Met801; Leu887; Tyr 890; Leu797;Cys891	Thr894; Asn719; Gln725
3	Genistein	Leu715; Leu718; Leu721; Phe778; Met759; Met801; Leu763; Leu797	Thr894; Asn719; Gln725
4	Myricetol	Leu715; Leu718; Leu721; Leu763; Phe778; Val760; Met759; Met801; Leu887;Tyr890; Leu797;Cys891	Thr894; Asn719; Gln725
5	Norethindrone Acetate	Leu718; Leu721; Leu763; Val760; Met759; Met801; Leu797; Leu887; Cys891	Thr894; Asn719; Gln725
6	Quercentin	Leu715; Leu718; Leu721; Leu763; Phe778; Val760; Met759; Met756; Met801; Leu887; Tyr890; Leu797; Thr890; Cys891	Thr894; Asn719; Gln 725
7	Tanshinone-I	Leu718; Leu721; Leu763; Phe778; Val760; Met759; Met756; Met801; Leu887; Tyr890; Leu797; Cys891	Thr894; Gln725

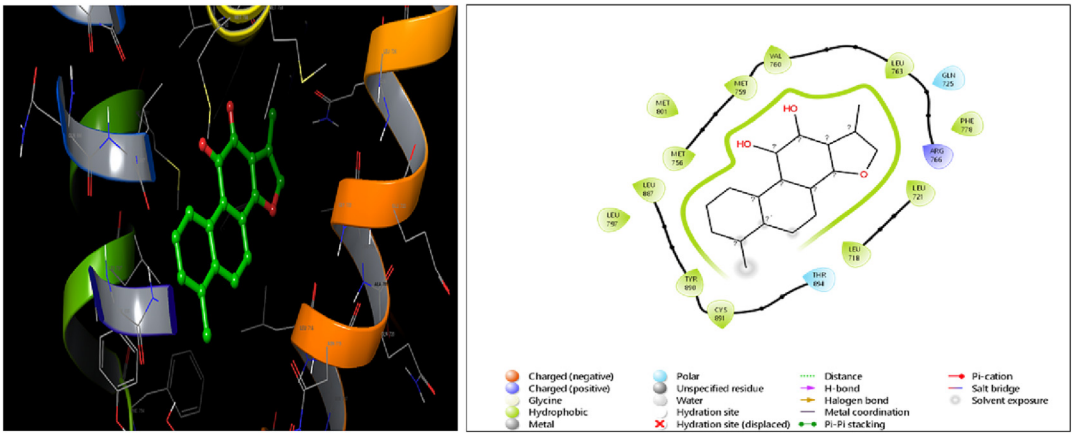

Fig. 5. 3d &2d- Docking interaction on 2OVH with Tanshinone-I.

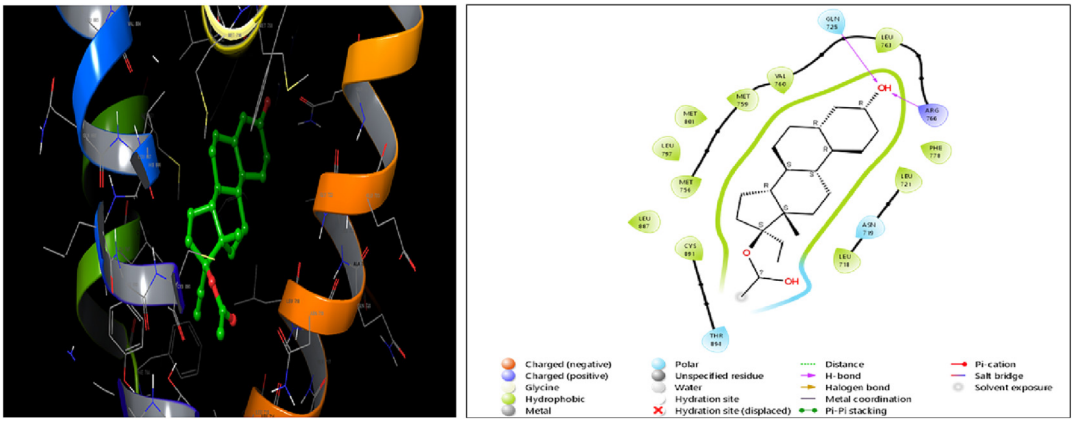

Fig. 6. 3d & 2d- Docking interaction on 2OVH with Norethindrone Acetate.

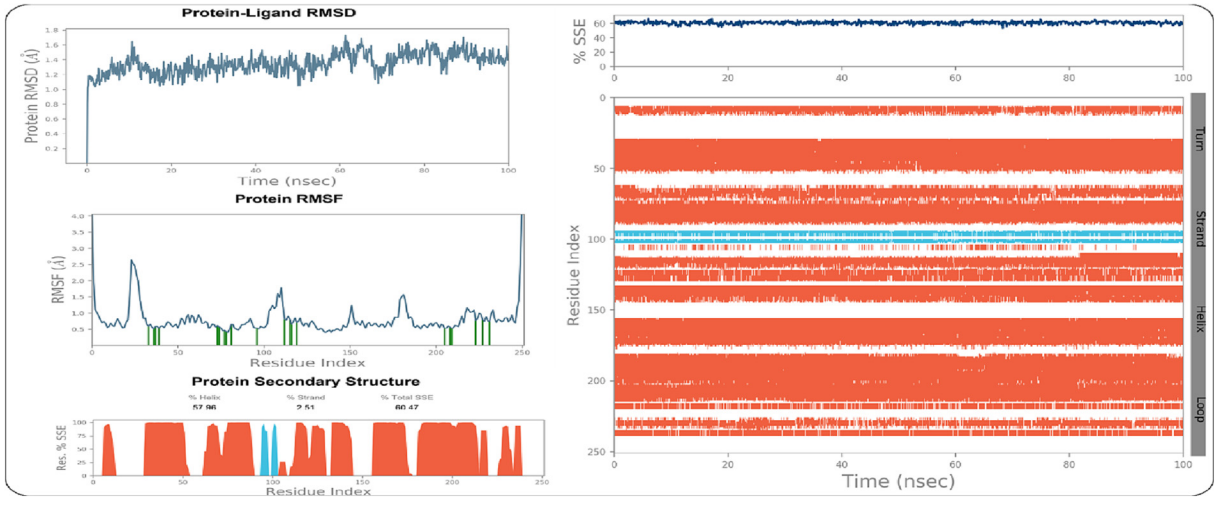

Fig. 7. Protein Ligand RMSD, RMSF, secondary structure of protein, % SSE and residue Index with 1E3K.

Tanshinone-I is virtually docked with 1E3K protein with a docking score of −10.2 kcal/mol and 13 rotatable bonds and affinities with amino acids like Val 760; Met 759; Met 756; Met 801; Leu 887; Tyr 890; Cys 891; Leu 715; Leu 718; Leu 72 (hydrophobic), Gln 725; Asn 719; Thr 894 (polar). This drug has shown a comparable docking score with the standard drug Norethindrone Acetate of −10.7 kcal/mol; 16 rotatable bonds and affinities with amino acids like Leu 763; Val 760; Met 759; Met 756; Met 801; Leu 887; Tyr 890; Cys 891; Leu 715; Phe 905; Phe 794; Leu 718; Met 909 (hydrophobic) and Gln 725; Asn 719; Thr 894 (polar). Similarly, with 2OVH, Tanshinone-I with a docking score of −9.9 kcal/mol is comparable to the standard, Norethindrone Acetate, (-10.1 kcal/mol); 16 rotatable bonds and affinities with amino acids such as Leu 718, Leu 721, Leu 763, Phe 778, Val 760,

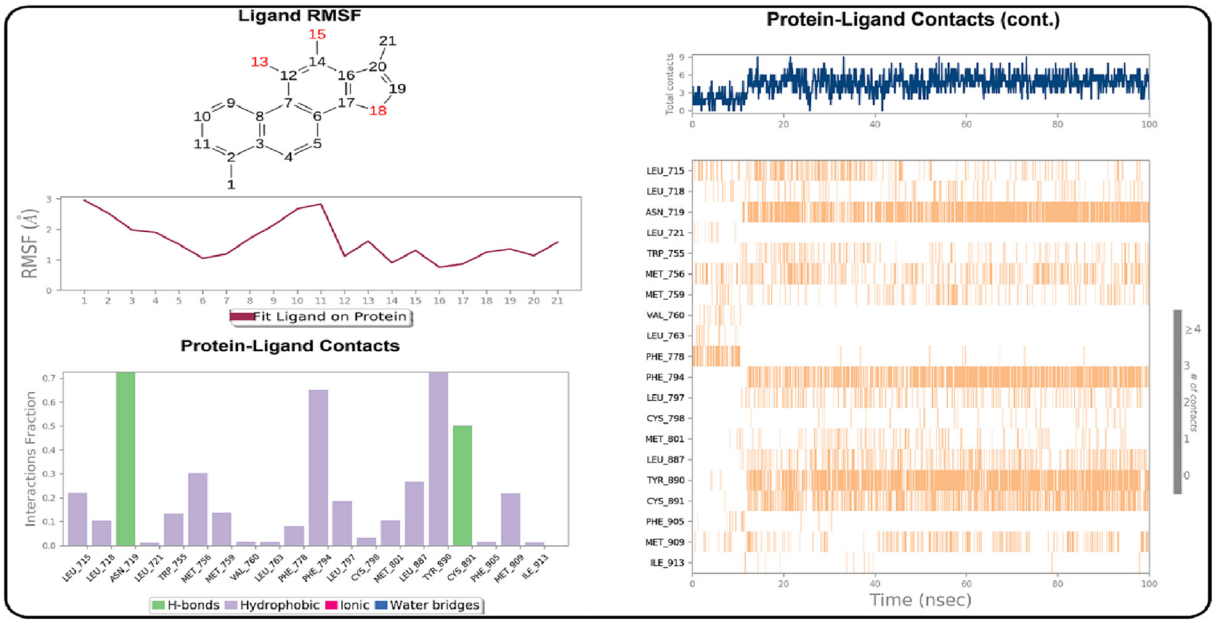

Fig. 8. Ligand RMSF and Protein Ligand Contacts for 100 ns with 1E3K protein.

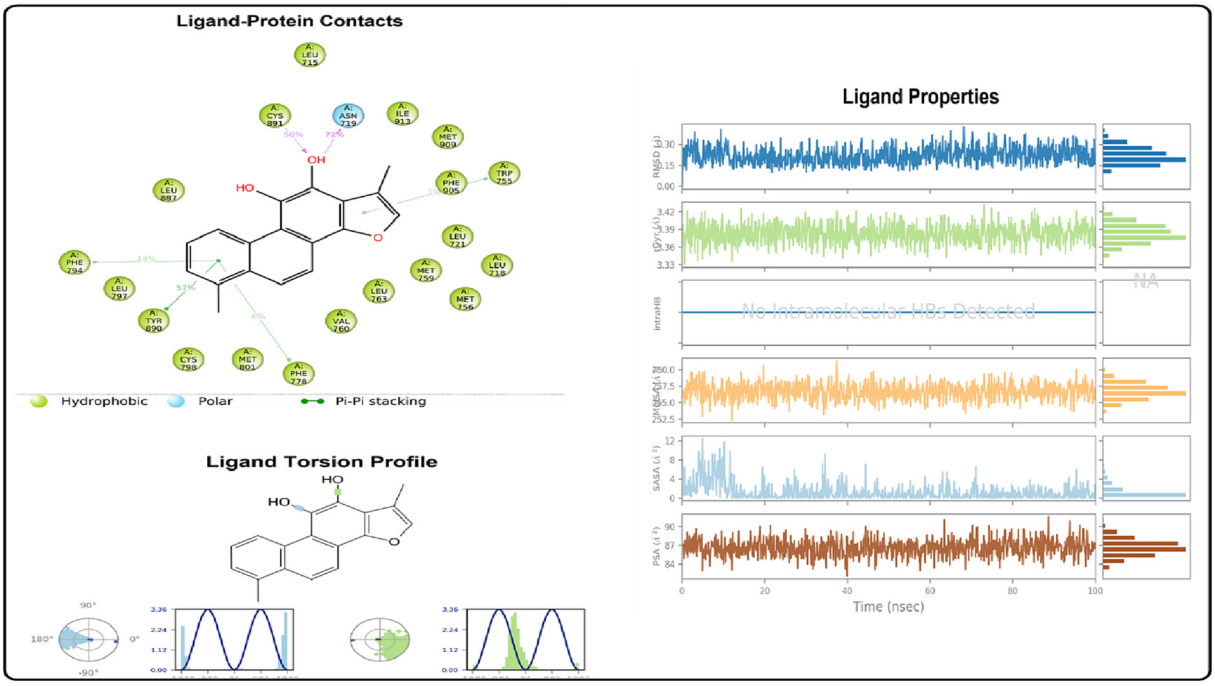

Fig. 9. Ligand-Protein contact with 1E3K and interaction with different amino acids, Tanshinone-I torsion profile and Properties (PSA, SASA, MolSA, rGyr and RMSD).

Met 759, Met 756, Met 801, Leu 887, Tyr 890, Leu 797, Cys 891 (hydrophobic) and Thr 894; Asn 719; Gln 725 (polar) (Si et al., 2009; Wu et al., 2005).

4.1. Molecular dynamics simulation

It is the best method to validate the docking score. Tanshinone-I was found to be the most potent drug against receptor 1E3K and 2OVH and showed the maximum docking score (-10.2 kcal/mol and −9.9 kcal/mol). The complex of protein with ligand has been simulated for 100 ns and found stable (Basu et al., 2020; El Ouafy et al., 2022).

RMSD and RMSF estimations have been performed to assess the trajectory generated following simulation, as shown in Fig. 7. The RMSD of the protein–ligand complex attained a minimum value of 0.10 Å and a maximum value of 0.42 Å with an average value of 0.21 Å between 100 ns and a standard deviation of 0.06. Rad gyration (rGyr) was found to be 3.33 Å with a mean value of 3.38 Å, and a standard deviation of 0.02 (Fig. 8). RMSF values have been estimated to assess the residue's mobility for conformational

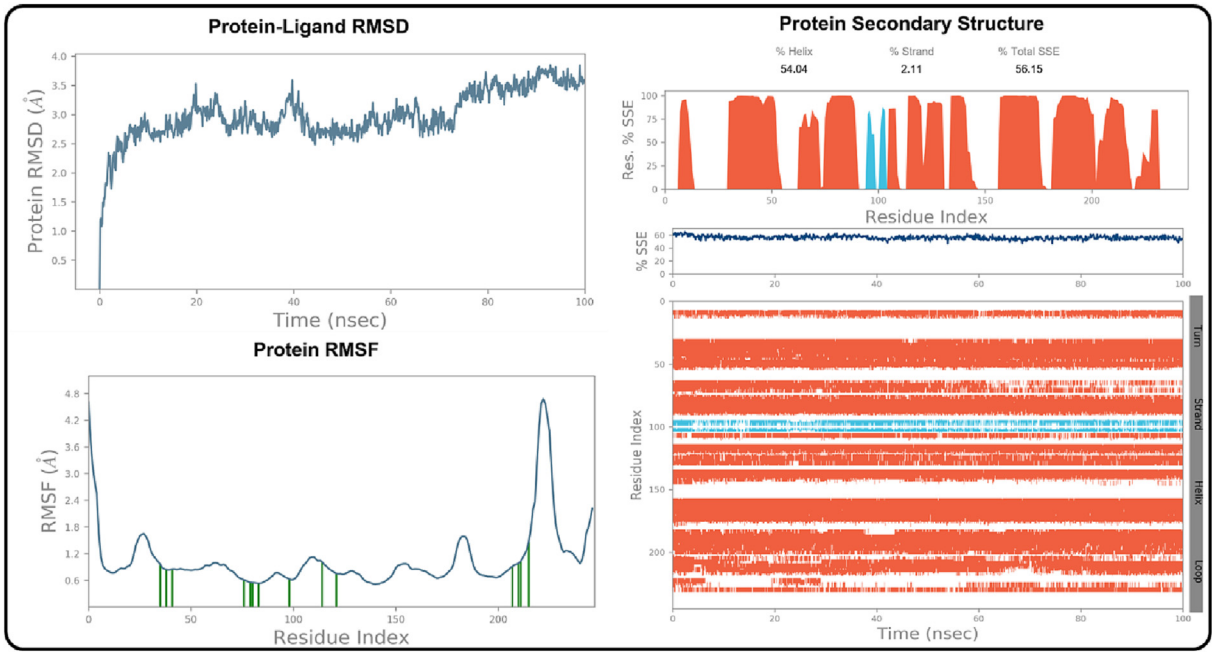

Fig. 10. Protein Ligand RMSD, secondary structure of protein % SSE and residue Index with 2OVH.

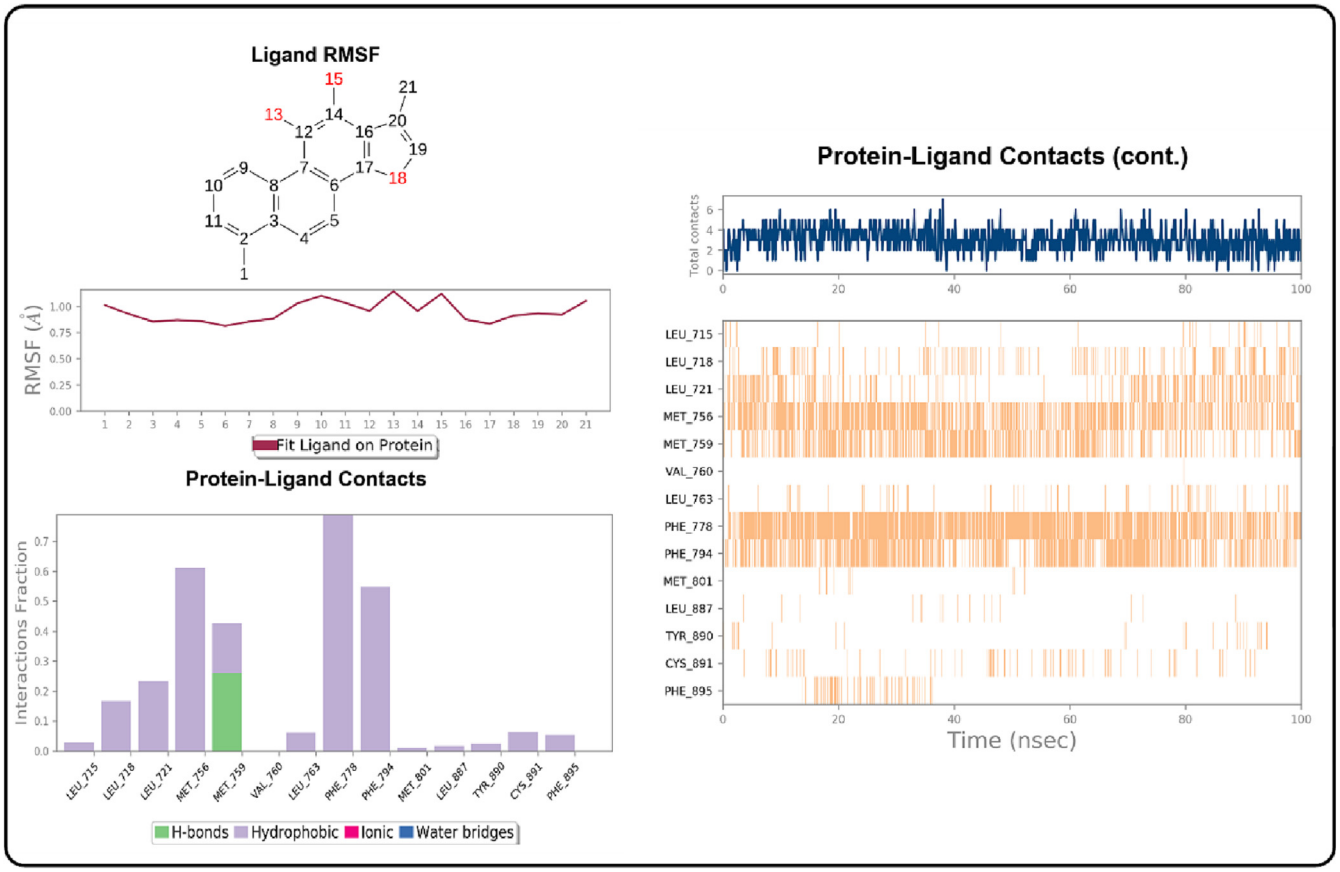

Fig. 11. Ligand RMSF and Protein Ligand Contacts with 2OVH.

alterations in complex-ligand interaction. The Vander Waals surface area (MolSA) was found to be 252.36 Å^2 with an average value of 256.70 Å^2 and a standard deviation of 1.20. The solvent accessible surface area (SASA) was found to be 12.34 Å^2 with an average value of 1.26 Å^2 and a standard deviation of 1.79. The molecular polar surface area (PSA) was found to be 82.10 Å^2 with an average value of 86.60 Å2 and standard deviation of 1.33. On the basis of the above analysis, the docked protein–ligand composite of 1E3K

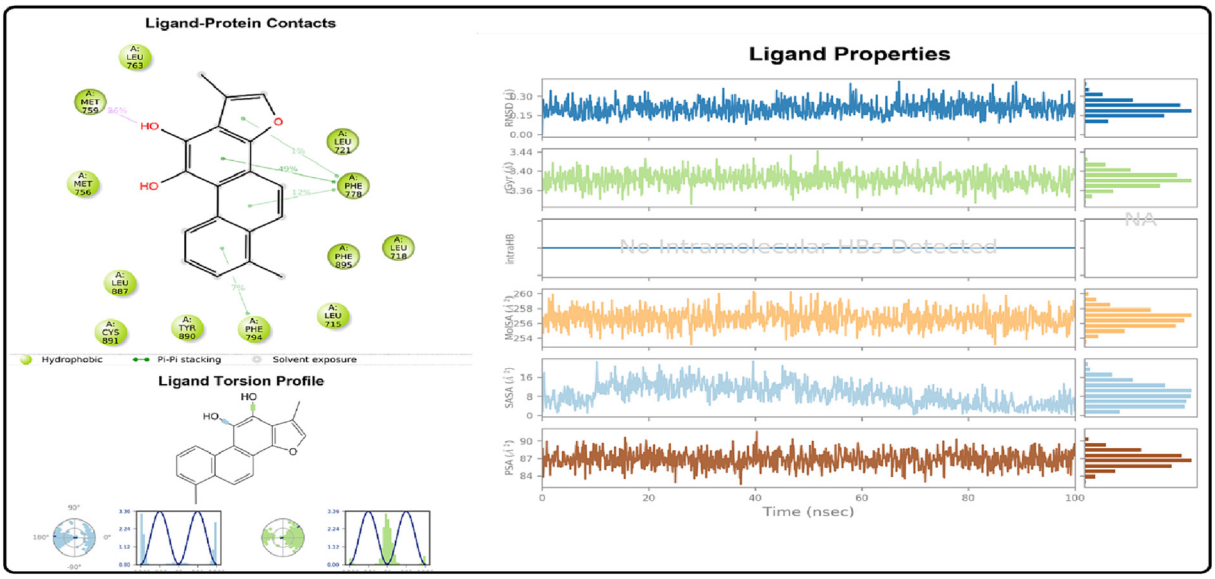

Fig. 12. Ligand-Protein contact with 2OVH and interaction with different amino acids, Tanshinone-I torsion profile and Properties (PSA, SASA, MolSA, rGyr and RMSD).

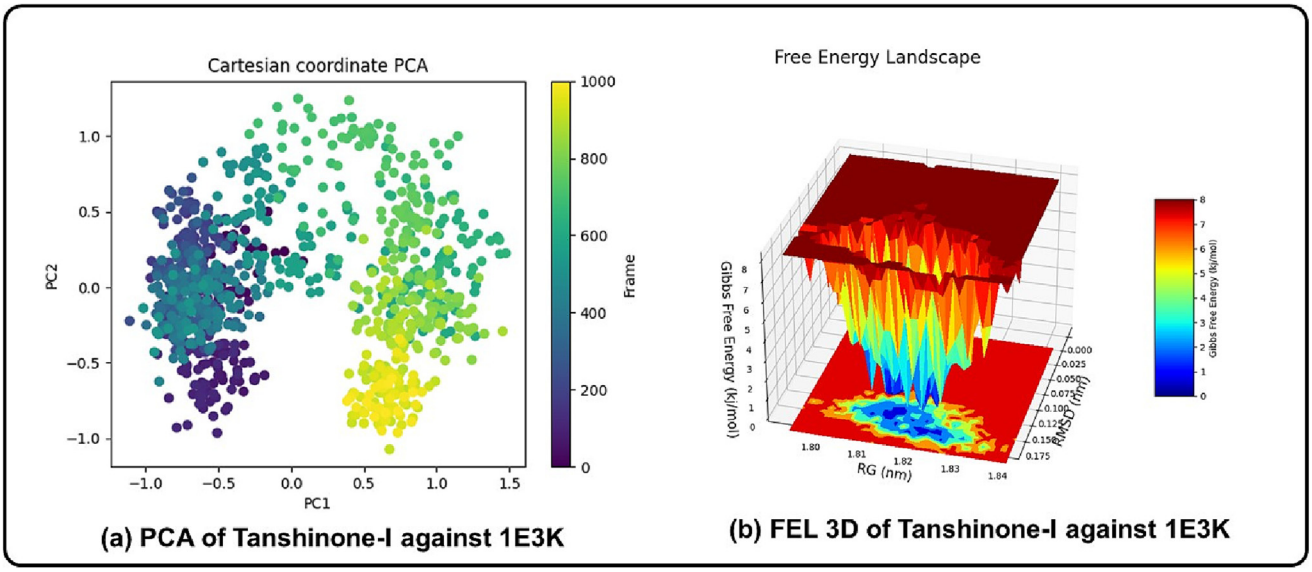

Fig. 13. Results of (a) Principle compnent analysis (b) FEL 3D for 1E3K.

with Tanshinone-I was found to be stable, and the docking result might be validated (Fig. 9). The protein secondary structure shows 57.96 % helix, 2.51 % strand, and 60.47 % protein secondary structure elements (SSE) (Fig. 7). Asn 719 and Cys 891 have shown the most hydrogen bonding, while Phe 794, Tyr 890, Arg 841 and Asp 855 had shown the most hydrophobic bonds. H-bonds have a mean value of 4.382 with a standard deviation of 0.974. There was no ionic or intramolecular hydrogen bond interaction. The torsion profile of ligands is shown in Fig. 9. This shows that there is no bond that can rotate at 3600 angles (Basu et al., 2020; El Ouafy et al., 2022).

Similarly, RMSD and RMSF calculations of Tanshinone-I with 2OVH are shown in Fig. 10. The RMSD of the protein–ligand complex was as low as 0.08 Å and as high as 0.42 Å, with an average value of 0.20 Å and a standard deviation of 0.06. rGyr was found to be 3.33 Å, with a mean value of 3.38 Å and a standard deviation of 0.02. (Fig. 11). RMSF values have been calculated to figure out how easily the residue can change shape if the complex and ligand interact. The average value of the MolSA was 256.62 Å2, and the standard deviation was 1.15. The average value of SASA was 8.83 Å2, and the standard deviation was 4.31. The average value of PSA was 86.84 Å2, and the standard deviation was 1.33. Based on the above analysis, the docked protein–ligand complex of 2OVH with Tanshinone-I was found to be stable, which means that the docking result could be confirmed (Fig. 12). There is 54.04% helix, 2.11% strand, and 56.15% SSE in the protein's secondary structure (Fig. 10). Most hydrophobic bonds were made by Phe778, Phe794, Leu721, and Leu718. Most hydrogen bonds were made by MET 759. There was no interaction between ions and molecules through hydrogen bonds. Fig. 11 shows the ligands' torsion profiles. This proves that there is no bond that can turn 3600 degrees (Basu et al., 2020; El Ouafy et al., 2022; Miar et al., 2021).

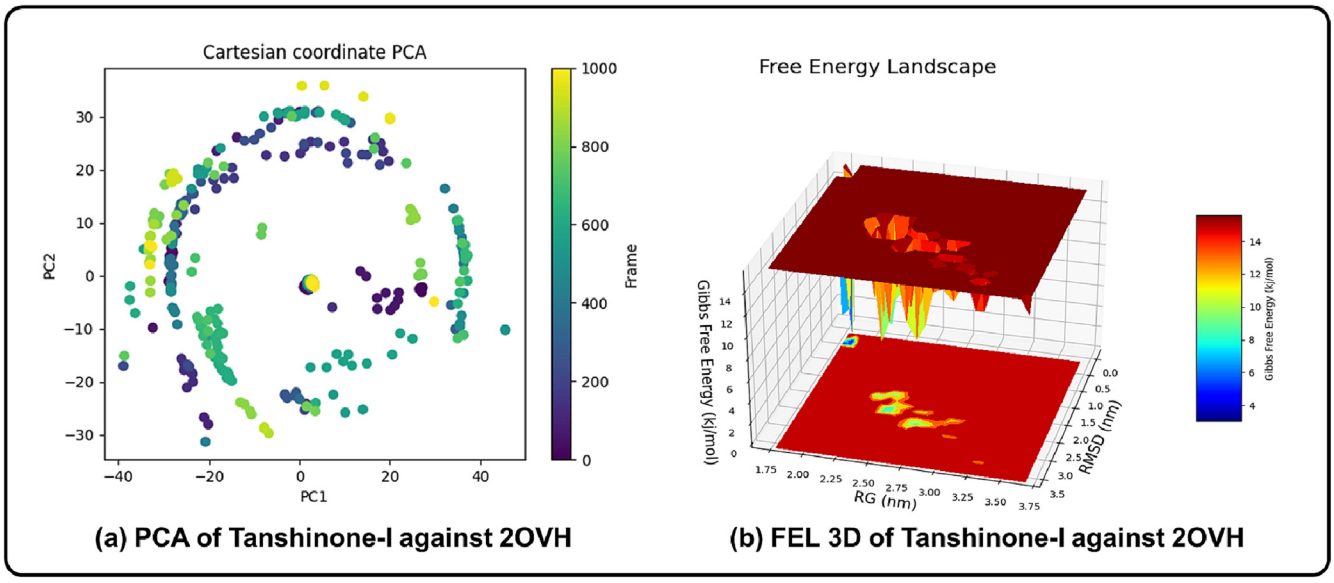

Fig. 14. Results of (a) Principle compnent analysis (b) FEL 3D for 2OVH.

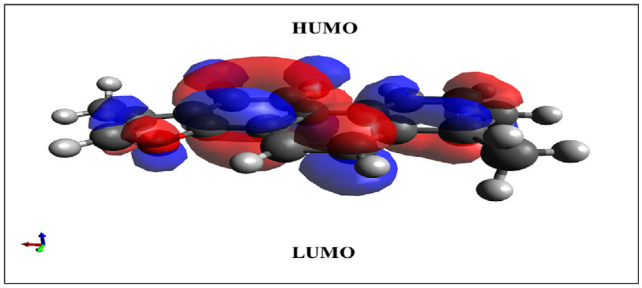

Fig. 15. Energy gap between HUMO and LUMO for Tanshinone-I.

Table 7
DFT analysis of Tanshinone-I.

S. No.	Calculation (eV)	Tanshinone-I (eV)
1.	E_{HOMO}	−5.9400
2.	E_{LUMO}	−3.1330
3.	ΔE	2.8070
4.	μ	−4.5365
5.	N	1.4035
6.	σ	0.7125
7.	I	5.9400
8.	A	3.1330
9.	χ	4.5365
10.	ω	7.3316
11.	ΔNmax	3.2323
12.	N	3.4286

4.2. Results of PCA analysis

The PCA reveals an overall increase in protein during the simulation; consequently, differences in dynamics were produced along each of the 1002 eigenvectors. PCs are responsible for a significant portion of the global motion of a protein. Two-directional movements of PCs, also known as the first eigen vector (PC1) and the second eigen vector (PC2), were investigated. In Fig. 13A, it can be observed that the eigen values of HPR-Tanshinone-I fluctuate between −1.11 to 1.48 and −1.07 to 1.25 for PC1 and PC2, respectively (1E3K), and in Fig. 14A, the prog-tanshinone-I complex shows eigen values of −38.88 to −31.32 and −31.32 to 35.87 for PC1 and PC2, respectively (2OVH). Overall, PCA results affirm that binding of the Tanshinone-I to 1E3K forms the most stable protein–ligand complex in comparison to Tanshinone-I to 2OVH (Dalal et al., 2021).

4.3. Results of FEL analysis

Tanshinone-I complexes show a higher number of stable conformations, as shown in Fig. 13B and 14B. Additionally, the Tanshinone-I to 1E3K complex showed Gibbs free energy in the range of 0 to 8 kJ/mol and the Tanshinone-I to 2OVH complex showed 0 to 14 kJ/mol. Moreover, 3D plots of free energy of Tanshinone-I to 1E3K and Tanshinone-I to 2OVH complexes were generated to determine the RMSD and RG for favorable conformations of the complexes. As shown in Fig. 13B and 14B. Tanshinone-I to 1E3K complex exhibits lesser RMSD and RG as compared to Tanshinone-I to 2OVH (Dalal et al., 2021).

4.4. DFT analysis

During molecular interactions, both the LUMO and the HOMO absorb electrons. The energy of the LUMO is related to the electron affinity (EA), while the energy of the HOMO is related to the ionization potential (IP). The HOMO-LUMO energy gap is helpful for figuring out how molecules can move electricity because it shows how the final charge transfer happens inside the molecule. A high orbital gap (HOMO-LUMO energy gap) means that it is energetically unfavorable to add an electron to the high-lying LUMO in order to remove electrons from the low-lying HOMO. This makes the molecule less reactive and more stable. Compounds that are more stable, like those with a large HOMO-LUMO energy gap, are less likely to change chemically than those with a smaller gap. Table 7 and Fig. 15 show that tanshinone-I (△E = 2.8070 eV) is a stable compound (Miar et al., 2021).

4.5. Possible mechanisms of selected best compound Tanshinone-I

Tanshinone I can cause ROS, apoptosis, autophagy (p62 accumulation), up-regulation of inositol requiring protein-1, enhancer-binding homologous protein, and p-c-Jun N-terminal kinase (p-JNK), and suppression of MMPs. B-cell leukemia/lymphoma-2 (Bcl-2) expression can change LC3I to LC3II and cause apoptosis through Beclin-1 expression (seven mechanisms as shown in Fig. 16). It also induced Aurora A-p53, and surviving, sig-

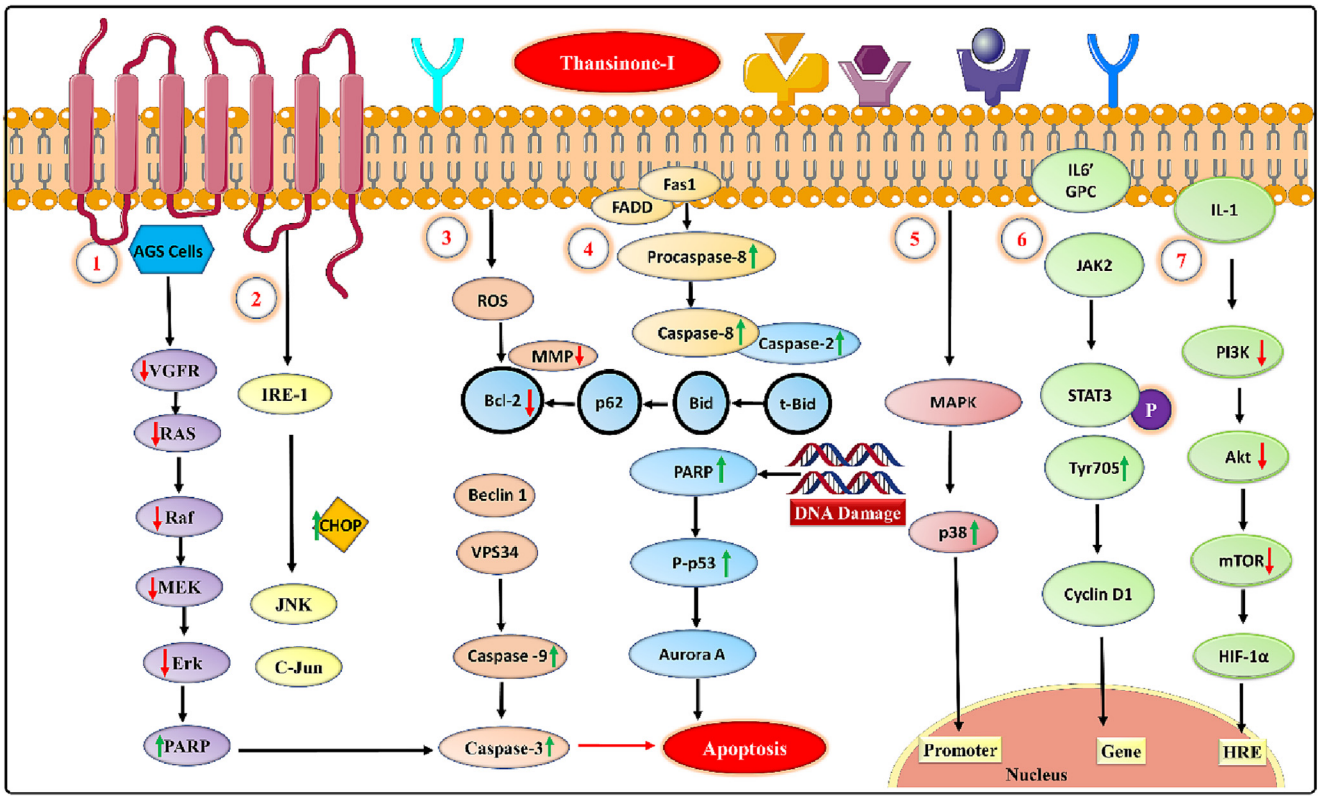

Fig. 16. Possible mechanism of Selected drug.

naling pathways lead to upregulation of PARP, which further stimulates p53 expression and reduces the Aurora A kinase level. Along with this, it also regulates caspase-3 and caspase-9, which in turn induce apoptosis in colorectal cancers. It also dissociates the procaspase-8 and suppresses the Bid, while t-Bid stimulates caspase-2. Through the downregulation of PI3K/Akt/m-TOR, breast cancer triggers apoptosis. It also acts through the MAPK pathway, which induces p38 to act as a promoter in the nucleus. Another pathway reported is JAK2, which further effects the gene through cyclin D1 and further stimulates the Tyr 70S. Another pathway involved is the downregulation of Bcl2 and MMP, which further promotes the degradation of nucleic acids in tumor cells (Naz et al., 2020; Taylor and Leppert, 2012; Pang et al., 2016; Gao et al., 2012; Kakisawa et al., 1969; Ma et al., 2015; Jang et al., 2003; Xu et al., 2018).

5. Conclusions

The present this research explores 28 phytochemicals and two different types of medicines were coupled to the 1E3K and 2OVH proteins. Tanshinone-I has demonstrated the highest level of activity for both of the proteins. Tanshinone-I has also been demonstrated through MD simulation research to form stable interactions with the receptors. In addition, the DFT study demonstrated that the molecule is not unstable. In general, these findings suggest that tanshinone-I might be useful as a medication in the treatment of fibroids. 1E3K is a steroidal agonist that modulates the prog pathway and can have an agonist or antagonistic effect on hPRs. Strong binding with 1E3K shows that it works to reduce the size of fibroid tumors instead of reducing heavy menstrual bleeding. Tanshinone-I with that of different ligands that bind to PR, such as full agonists and SPRMs. Even small changes to the structure of the parent molecule can make a big difference in how the derivative works. Non-steroidal SPERMs are being made all the time, like the recently reported 3-aryl indoles. Due to the fact that it works in different ways against different types of cancer, this drug has the potential to solve the problem either on its own or in combination with other drugs. Tanshinone-I may be the focus of future drug development strategies for fibroids.

CRediT authorship contribution statement

Abhishek Tiwari: Writing – review & editing, Writing – original draft, Software, Conceptualization. **Varsha Tiwari:** Writing – original draft, Software, Conceptualization. **Ajay Sharma:** Software. **Deependra Singh:** Writing – original draft. **Manju Singh Rawat:** Writing – original draft. **Manish Kumar:** Writing – review & editing. **Abdulsalam Alhalmi:** Writing – review & editing. **Tarun Virmani:** Writing -review & editing. **Girish Mittal:** Writing -review & editing. **Resu Virmani:** Writing -review & editing. **Ramzi A.Mothana:** Writing -review & editing. **Omar M. Noman:** Writing -review & editing. **Mohammad Alali S:** Writing -review & editing.

Declaration of Competing Interest

The authors declare that they have no known competing financial interests or personal relationships that could have appeared to influence the work reported in this paper.

Acknowledgments

The authors extend their appreciation to Researchers Supporting Project number (RSP2023R119), King Saud University, Riyadh, Saudi Arabia for funding this work.

Funding

This research was funded by to Researchers Supporting Project number (RSP2023R119), King Saud University, Riyadh, Saudi Arabia

Appendix A. Supplementary data

Supplementary data to this article can be found online at https://doi.org/10.1016/j.jsps.2023.05.002.

References

Al-Hendy, A., Bradley, L., Owens, C.D., Wang, H., Barnhart, K.T., Feinberg, E., Schlaff, W.D., Puscheck, E.E., Wang, A., Gillispie, V., Hurtado, S., Muneyyirci-Delale, O., Archer, D.F., Carr, B.R., Simon, J.A., Stewart, E.A., 2021. Predictors of response for elagolix with add-back therapy in women with heavy menstrual bleeding associated with uterine fibroids. Am. J. Obstet. Gynecol. 224, 72.e1–72.e50. https://doi.org/10.1016/j.ajog.2020.07.032.

Alshatwi, A.A., 2010. Catechin hydrate suppresses MCF-7 proliferation through TP53/Caspase-mediated apoptosis. J. Exp. Clin. Cancer Res. 29, 167. https://doi.org/10.1186/1756-9966-29-167.

An, M., Kim, M., 2015. Protective effects of kaempferol against cardiac sinus node dysfunction via CaMKII deoxidization. Anat. Cell Biol. 48, 235–243. https://doi.org/10.5115/acb.2015.48.4.235.

Angelis, A., Hubert, J., Aligiannis, N., Michalea, R., Abedini, A., Nuzillard, J.-M., Gangloff, S.C., Skaltsounis, A.-L., Renault, J.-H., 2016. Bio-Guided Isolation of Methanol-Soluble Metabolites of Common Spruce (Picea abies) Bark by-Products and Investigation of Their Dermo-Cosmetic Properties. Molecules 21. https://doi.org/10.3390/molecules21111586.

Ansari, M.A., Khan, F.B., Safdari, H.A., Almatroudi, A., Alzohairy, M.A., Safdari, M., Amirizadeh, M., Rehman, S., Equbal, M.J., Hoque, M., 2021. Prospective therapeutic potential of Tanshinone IIA: An updated overview. Pharmacol. Res. 164, 105364. https://doi.org/10.1016/j.phrs.2020.105364.

Axelson, M., Kirk, D.N., Farrant, R.D., Cooley, G., Lawson, A.M., Setchell, K.D., 1982. The identification of the weak oestrogen equol [7-hydroxy-3-(4'-hydroxyphenyl)chroman] in human urine. Biochem. J. 201, 353–357. https://doi.org/10.1042/bj2010353.

Basu, A., Sarkar, A., Maulik, U., 2020. Molecular docking study of potential phytochemicals and their effects on the complex of SARS-CoV2 spike protein and human ACE2. Sci. Rep. 10, 17699. https://doi.org/10.1038/s41598-020-74715-4.

Boonyaratanakornkit, V., Scott, M.P., Ribon, V., Sherman, L., Anderson, S.M., Maller, J. L., Miller, W.T., Edwards, D.P., 2001. Progesterone receptor contains a proline-rich motif that directly interacts with SH3 domains and activates c-Src family tyrosine kinases. Mol. Cell 8, 269–280. https://doi.org/10.1016/s1097-2765(01)00304-5.

Boonyaratanakornkit, V., Edwards, D.P., 2007. Receptor mechanisms mediating non-genomic actions of sex steroids. Semin. Reprod. Med. 25, 139–153. https://doi.org/10.1055/s-2007-973427.

Bowers, K.J., Chow, E., Xu, H., Dror, R.O., Eastwood, M.P., Gregersen, B.A., Klepeis, J.L., Kolossvary, I., Moraes, M.A., Sacerdoti, F.D., Salmon, J.K., Shan, Y., Shaw, D.E., 2006. Scalable algorithms for molecular dynamics simulations on commodity clusters. In: Proceedings of the 2006 ACM/IEEE Conference on Supercomputing, SC'06. https://doi.org/10.1145/1188455.1188544.

Cheng, J.-C., Kan, L.-S., Chen, J.-T., Chen, L.-G., Lu, H.-C., Lin, S.-M., Wang, S.-H., Yang, K.-H., Chiou, R.-Y.-Y., 2009. Detection of cyanidin in different-colored peanut testae and identification of peanut cyanidin 3-sambubioside. J. Agric. Food Chem. 57, 8805–8811. https://doi.org/10.1021/jf902512k.

Cheng, D.C., Wolfe, B.M., 1983. Norethindrone acetate inhibition of triglyceride synthesis and release by rat hepatocytes. Atherosclerosis 46, 41–48. https://doi.org/10.1016/0021-9150(83)90162-4.

Cheruku, S.P., Ramalingayya, G.V., Chamallamudi, M.R., Biswas, S., Nandakumar, K., Nampoothiri, M., Gourishetti, K., Kumar, N., 2018. Catechin ameliorates doxorubicin-induced neuronal cytotoxicity in in vitro and episodic memory deficit in in vivo in Wistar rats. Cytotechnology 70, 245–259. https://doi.org/10.1007/s10616-017-0138-8.

Chiou, Y.-S., Ma, N.-J.-L., Sang, S., Ho, C.-T., Wang, Y.-J., Pan, M.-H., 2012. Peracetylated (-)-epigallocatechin-3-gallate (AcEGCG) potently suppresses dextran sulfate sodium-induced colitis and colon tumorigenesis in mice. J. Agric. Food Chem. 60, 3441–3451. https://doi.org/10.1021/jf300441p.

Choi, Y.R., Shim, J., Kim, M.J., 2020. Genistin: A Novel Potent Anti-Adipogenic and Anti-Lipogenic Agent. Molecules 25. https://doi.org/10.3390/molecules25092042.

Chung, S.S., Vadgama, J.V., 2015. Curcumin and epigallocatechin gallate inhibit the cancer stem cell phenotype via down-regulation of STAT3-NFκB signaling. Anticancer Res. 35, 39–46.

Czarnik, M., Cusimano, F.A., Bahlani, S., Ciuffo, N., Vaglica, A., Mitchell, C., Ziffer, C., Hernandez, G., Gentile, N., Watkins, A., Tonis, A., Greuner, D.A., 2023. Embolization for the treatment of large, complex fibroids in an outpatient setting: A report of 2 cases. Radiol. Case Reports 18, 936–942. https://doi.org/10.1016/j.radcr.2022.11.036.

Dalal, V., Dhankhar, P., Singh, V., Singh, V., Rakhaminov, G., Golemi-Kotra, D., Kumar, P., 2021. Structure-Based Identification of Potential Drugs Against FmtA of Staphylococcus aureus: Virtual Screening, Molecular Dynamics, MM-GBSA, and QM/MM. Protein J. 40, 148–165. https://doi.org/10.1007/s10930-020-09953-6.

Dalton-Brewer, N., 2016. The Role of Complementary and Alternative Medicine for the Management of Fibroids and Associated Symptomatology. Curr. Obstet. Gynecol. Rep. 5, 110–118. https://doi.org/10.1007/s13669-016-0156-0.

Don, E.E., Mijatovic, V., van Eekelen, R., Huirne, J.A.F., 2022. The effect of myomectomy on reproductive outcomes in patients with uterine fibroids: A retrospective cohort study. Reprod. Biomed. Online 45, 970–978. https://doi.org/10.1016/j.rbmo.2022.05.025.

Du, G.-J., Zhang, Z., Wen, X.-D., Yu, C., Calway, T., Yuan, C.-S., Wang, C.-Z., 2012. Epigallocatechin Gallate (EGCG) is the most effective cancer chemopreventive polyphenol in green tea. Nutrients 4, 1679–1691. https://doi.org/10.3390/nu4111679.

El Ouafy, H., Aamor, M., Oubenali, M., Mbarki, M., El Haimouti, A., El Ouafy, T., 2022. Molecular Structure, Electrostatic Potential and HOMO, LUMO Studies of 4-Aminoan-iline, 4-Nitroaniline and 4-Isopropylaniline by DFT. Sci. Technol. Asia 27, 9–19 https://doi.org/10.14456/scitechasia.2022.2.

Gao, S., Liu, Z., Li, H., Little, P.J., Liu, P., Xu, S., 2012. Cardiovascular actions and therapeutic potential of tanshinone IIA. Atherosclerosis 220, 3–10. https://doi.org/10.1016/j.atherosclerosis.2011.06.041.

Hu, S., Huang, L., Meng, L., Sun, H., Zhang, W., Xu, Y., 2015. Isorhamnetin inhibits cell proliferation and induces apoptosis in breast cancer via Akt and mitogen-activated protein kinase kinase signaling pathways. Mol. Med. Rep. 12, 6745–6751. https://doi.org/10.3892/mmr.2015.4269.

Hwang, S.T., Yang, M.H., Baek, S.H., Um, J.-Y., Ahn, K.S., 2020. Genistin attenuates cellular growth and promotes apoptotic cell death breast cancer cells through modulation of ERalpha signaling pathway. Life Sci. 263,. https://doi.org/10.1016/j.lfs.2020.118594 118594.

Ignasimuthu, K., Prakash, R., Murthy, P.S., Subban, N., 2019. Enhanced bioaccessibility of green tea polyphenols and lipophilic activity of EGCG octaacetate on gram-negative bacteria. LWT 105, 103–109. https://doi.org/10.1016/J.LWT.2019.01.064.

Jang, S.-I., Jeong, S.-I., Kim, K.-J., Kim, H.-J., Yu, H.-H., Park, R., Kim, H.-M., You, Y.-O., 2003. Tanshinone IIA from Salvia miltiorrhiza inhibits inducible nitric oxide synthase expression and production of TNF-alpha, IL-1beta and IL-6 in activated RAW 264.7 cells. Planta Med. 69, 1057–1059. https://doi.org/10.1055/s-2003-45157.

Jinwal, U.K., Miyata, Y., Koren 3rd, J., Jones, J.R., Trotter, J.H., Chang, L., O'Leary, J., Morgan, D., Lee, D.C., Shults, C.L., Rousaki, A., Weeber, E.J., Zuiderweg, E.R.P., Gestwicki, J.E., Dickey, C.A., 2009. Chemical manipulation of hsp70 ATPase activity regulates tau stability. J. Neurosci. Off. J. Soc. Neurosci. 29, 12079–12088. https://doi.org/10.1523/JNEUROSCI.3345-09.2009.

Kakisawa, H., Hayashi, T., Yamazaki, T., 1969. Structures of isotanshinones. Tetrahedron Lett. 10, 301–304. https://doi.org/10.1016/S0040-4039(01)87676-0.

Kannan, S., Kolandaivel, P., 2018. The inhibitory performance of flavonoid cyanidin-3-sambubiocide against H274Y mutation in H1N1 influenza virus. J. Biomol. Struct. Dyn. 36, 4255–4269. https://doi.org/10.1080/07391102.2017.1413422.

Kannen, V., Garcia, S.B., Stopper, H., Waaga-Gasser, A.M., 2013. Glucagon-like peptide 2 in colon carcinogenesis: possible target for anti-cancer therapy?. Pharmacol. Ther. 139, 87–94. https://doi.org/10.1016/j.pharmthera.2013.04.007.

Keizer, A.L., Jacobs, B.L., Thurkow, A.L., de Lange, M.E., Radder, C.M., van Kesteren, P. J.M., Hanstede, M.M.F., Huirne, J.A.F., Hehenkamp, W.J.K., 2022. The effect of transcervical resection of submucous fibroids on menstrual blood loss: A prospective cohort study. Eur. J. Obstet. Gynecol. Reprod. Biol. 274, 128–135. https://doi.org/10.1016/j.ejogrb.2022.05.019.

Kellis, J.T.J., Vickery, L.E., 1984. Inhibition of human estrogen synthetase (aromatase) by flavones. Science 225, 1032–1034. https://doi.org/10.1126/science.6474163.

Khandelwal, N., Abraham, S.K., 2014. Intake of anthocyanidins pelargonidin and cyanidin reduces genotoxic stress in mice induced by diepoxybutane, urethane and endogenous nitrosation. Environ. Toxicol. Pharmacol. 37, 837–843. https://doi.org/10.1016/j.etap.2014.02.012.

Kim, S.C., Kim, Y.H., Son, S.W., Moon, E.-Y., Pyo, S., Um, S.H., 2015b. Fisetin induces Sirt1 expression while inhibiting early adipogenesis in 3T3-L1 cells. Biochem. Biophys. Res. Commun. 467, 638–644. https://doi.org/10.1016/j.bbrc.2015.10.094.

Kim, J.-E., Lee, D.-E., Lee, K.W., Son, J.E., Seo, S.K., Li, J., Jung, S.K., Heo, Y.-S., Mottamal, M., Bode, A.M., Dong, Z., Lee, H.J., 2011. Isorhamnetin suppresses skin cancer through direct inhibition of MEK1 and PI3-K. Cancer Prev. Res. (Phila) 4, 582–591. https://doi.org/10.1158/1940-6207.CAPR-11-0032.

Kim, E., Woo, M.-S., Qin, L., Ma, T., Beltran, C.D., Bao, Y., Bailey, J.A., Corbett, D., Ratan, R.R., Lahiri, D.K., Cho, S., 2015a. Daidzein Augments Cholesterol Homeostasis via ApoE to Promote Functional Recovery in Chronic Stroke. J. Neurosci. Off. J. Soc. Neurosci. 35, 15113–15126. https://doi.org/10.1523/JNEUROSCI.2890-15.2015.

Lee, S.-J., Hong, S., Yoo, S.-H., Kim, G.-W., 2013. Cyanidin-3-O-sambubioside from Acanthopanax sessiliflorus fruit inhibits metastasis by downregulating MMP-9 in breast cancer cells MDA-MB-231. Planta Med. 79, 1636–1640. https://doi.org/10.1055/s-0033-1350954.

Lee, H.J., Norwitz, E.R., Shaw, J., 2010. Contemporary management of fibroids in pregnancy. Rev. Obstet. Gynecol. 3, 20–27.

Lee, P., Tan, K.S., 2015. Effects of Epigallocatechin gallate against Enterococcus faecalis biofilm and virulence. Arch. Oral Biol. 60, 393–399. https://doi.org/10.1016/j.archoralbio.2014.11.014.

Leonhardt, S.A., Boonyaratanakornkit, V., Edwards, D.P., 2003. Progesterone receptor transcription and non-transcription signaling mechanisms. Steroids 68, 761–770. https://doi.org/10.1016/s0039-128x(03)00129-6.

Liang, Y., Zhao, W., Wang, C., Wang, Z., Wang, Z., Zhang, J., 2018. A Comprehensive Screening and Identification of Genistin Metabolites in Rats Based on Multiple Metabolite Templates Combined with UHPLC-HRMS Analysis. Molecules 23. https://doi.org/10.3390/molecules23081862.

Liu, T., Yang, Q., Zhang, X., Qin, R., Shan, W., Zhang, H., Chen, X., 2020. Quercetin alleviates kidney fibrosis by reducing renal tubular epithelial cell senescence through the SIRT1/PINK1/mitophagy axis. Life Sci. 257,. https://doi.org/10.1016/j.lfs.2020.118116 118116.

Luo, H., Rankin, G.O., Li, Z., Depriest, L., Chen, Y.C., 2011. Kaempferol induces apoptosis in ovarian cancer cells through activating p53 in the intrinsic pathway. Food Chem. 128, 513–519. https://doi.org/10.1016/j.foodchem.2011.03.073.

Luo, H., Jiang, B., Li, B., Li, Z., Jiang, B.-H., Chen, Y.C., 2012. Kaempferol nanoparticles achieve strong and selective inhibition of ovarian cancer cell viability. Int. J. Nanomedicine 7, 3951–3959. https://doi.org/10.2147/IJN.S33670.

Ma, X.-H., Ma, Y., Tang, J.-F., He, Y.-L., Liu, Y.-C., Ma, X.-J., Shen, Y., Cui, G.-H., Lin, H.-X., Rong, Q.-X., Guo, J., Huang, L.-Q., 2015. The Biosynthetic Pathways of Tanshinones and Phenolic Acids in Salvia miltiorrhiza. Molecules 20, 16235–16254. https://doi.org/10.3390/molecules200916235.

Miar, M., Shiroudi, A., Pourshamsian, K., Oliaey, A.R., Hatamjafari, F., 2021. Theoretical investigations on the HOMO–LUMO gap and global reactivity descriptor studies, natural bond orbital, and nucleus-independent chemical shifts analyses of 3-phenylbenzo[d]thiazole-2(3H)-imine and its para-substituted derivatives: Solvent and subs. J. Chem. Res. 45, 147–158. https://doi.org/10.1177/1747519820932091.

Mukhtar, E., Adhami, V.M., Sechi, M., Mukhtar, H., 2015. Dietary flavonoid fisetin binds to β-tubulin and disrupts microtubule dynamics in prostate cancer cells. Cancer Lett. 367, 173–183. https://doi.org/10.1016/j.canlet.2015.07.030.

Muneyyirci-Delale, O., Karacan, M., 1998. Effect of norethindrone acetate in the treatment of symptomatic endometriosis. Int. J. Fertil. Womens. Med. 43, 24–27.

Navarro-Núñez, L., Lozano, M.L., Martínez, C., Vicente, V., Rivera, J., 2010. Effect of quercetin on platelet spreading on collagen and fibrinogen and on multiple platelet kinases. Fitoterapia 81, 75–80. https://doi.org/10.1016/j.fitote.2009.08.006.

Naz, I., Merarchi, M., Ramchandani, S., Khan, M.R., Malik, M.N., Sarwar, S., Narula, A. S., Ahn, K.S., 2020. An overview of the anti-cancer actions of Tanshinones, derived from Salvia miltiorrhiza (Danshen). Explor. Target Antitumor. Ther. 1 (3), 153–170. https://doi.org/10.37349/etat.2020.00010.

Nogueira, L., Ramirez-Sanchez, I., Perkins, G.A., Murphy, A., Taub, P.R., Ceballos, G., Villarreal, F.J., Hogan, M.C., Malek, M.H., 2011. (-)-Epicatechin enhances fatigue resistance and oxidative capacity in mouse muscle. J. Physiol. 589, 4615–4631. https://doi.org/10.1113/jphysiol.2011.209924.

Ohguchi, K., Tanaka, T., Iliya, I., Ito, T., Iinuma, M., Matsumoto, K., Akao, Y., Nozawa, Y., 2003. Gnetol as a potent tyrosinase inhibitor from genus Gnetum. Biosci. Biotechnol. Biochem. 67, 663–665. https://doi.org/10.1271/bbb.67.663.

Okesola, M.A., Adegboyega, A.E., Lasisi, A.J., Bello, F.A., Ogunlana, O.O., Afolabi, I.S., 2022. Elucidating the interactions of bioactive compounds identified from Camellia Sinensis plant as promising candidates for the management of fibroids - A computational approach. Informatics Med. Unlocked 31,. https://doi.org/10.1016/j.imu.2022.101002 101002.

Pang, H., Wu, L., Tang, Y., Zhou, G., Qu, C., Duan, J., 2016. Chemical Analysis of the Herbal Medicine Salviae miltiorrhizae Radix et Rhizoma (Danshen). Molecules 21, 51. https://doi.org/10.3390/molecules21010051.

Patel, B., Elguero, S., Thakore, S., Dahoud, W., Bedaiwy, M., Mesiano, S., 2015. Role of nuclear progesterone receptor isoforms in uterine pathophysiology. Hum. Reprod. Update 21, 155–173. https://doi.org/10.1093/humupd/dmu056.

Phillips, P.A., Sangwan, V., Borja-Cacho, D., Dudeja, V., Vickers, S.M., Saluja, A.K., 2011. Myricetin induces pancreatic cancer cell death via the induction of apoptosis and inhibition of the phosphatidylinositol 3-kinase (PI3K) signaling pathway. Cancer Lett. 308, 181–188. https://doi.org/10.1016/j.canlet.2011.05.002.

Piriyev, E., Römer, T., 2023. Delayed expulsion of a large fibroid after transcervical radiofrequency ablation: A case report. Radiol. Case Reports 18, 779–783. https://doi.org/10.1016/j.radcr.2022.11.063.

Yudha Pratama Putra, P., Prameswari, A.S., Ma'roef, M., Musyarrofah, A., Nelasari, H., 2021. Laparoscopic myomectomy versus open myomectomy in uterine fibroid treatment: A meta-analysis. Laparosc. Endosc. Robot. Surg. 4, 66–71. https://doi.org/10.1016/j.lers.2021.08.002.

Raffort, J., Lareyre, F., Massalou, D., Fénichel, P., Panaïa-Ferrari, P., Chinetti, G., 2017. Insights on glicentin, a promising peptide of the proglucagon family. Biochem. medica 27, 308–324 https://doi.org/10.11613/BM.2017.034.

Ren, L., Guo, H.-N., Yang, J., Guo, X.-Y., Wei, Y.-S., Yang, Z., 2020. Dissecting Efficacy and Metabolic Characteristic Mechanism of Taxifolin on Renal Fibrosis by Multivariate Approach and Ultra-Performance Liquid Chromatography Coupled With Mass Spectrometry-Based Metabolomics Strategy. Front. Pharmacol. 11,. https://doi.org/10.3389/fphar.2020.608511 608511.

Sakamoto, Y., Kanatsu, J., Toh, M., Naka, A., Kondo, K., Iida, K., 2016. The Dietary Isoflavone Daidzein Reduces Expression of Pro-Inflammatory Genes through PPARα/γ and JNK Pathways in Adipocyte and Macrophage Co-Cultures. PLoS One 11, e0149676.

Saponara, S., Testai, L., Iozzi, D., Martinotti, E., Martelli, A., Chericoni, S., Sgaragli, G., Fusi, F., Calderone, V., 2006. (+/-)-Naringenin as large conductance Ca(2+)-activated K+ (BKCa) channel opener in vascular smooth muscle cells. Br. J. Pharmacol. 149, 1013–1021. https://doi.org/10.1038/sj.bjp.0706951.

Saritha, F., Aiswarya, N., Aswath Kumar, R., Dileep, K.V., 2023. Structural analysis and ensemble docking revealed the binding modes of selected prog receptor modulators. J. Biomol. Struct. Dyn. 1–10. https://doi.org/10.1080/07391102.2023.2166999.

Semwal, D.K., Semwal, R.B., Combrinck, S., Viljoen, A., 2016. Myricetin: A Dietary Molecule with Diverse Biological Activities. Nutrients 8, 90. https://doi.org/10.3390/nu8020090.

Setchell, K.D.R., Clerici, C., Lephart, E.D., Cole, S.J., Heenan, C., Castellani, D., Wolfe, B. E., Nechemias-Zimmer, L., Brown, N.M., Lund, T.D., Handa, R.J., Heubi, J.E., 2005. S-equol, a potent ligand for estrogen receptor beta, is the exclusive enantiomeric form of the soy isoflavone metabolite produced by human intestinal bacterial flora. Am. J. Clin. Nutr. 81, 1072–1079. https://doi.org/10.1093/ajcn/81.5.1072.

Shay, J., Elbaz, H.A., Lee, I., Zielske, S.P., Malek, M.H., Hüttemann, M., 2015. Molecular Mechanisms and Therapeutic Effects of (-)-Epicatechin and Other Polyphenols in Cancer, Inflammation, Diabetes, and Neurodegeneration. Oxid. Med. Cell. Longev. 2015,. https://doi.org/10.1155/2015/181260 181260.

Shin, D., Park, S.-H., Choi, Y.-J., Kim, Y.-H., Antika, L.D., Habibah, N.U., Kang, M.-K., Kang, Y.-H., 2015. Dietary Compound Kaempferol Inhibits Airway Thickening Induced by Allergic Reaction in a Bovine Serum Albumin-Induced Model of Asthma. Int. J. Mol. Sci. 16, 29980–29995. https://doi.org/10.3390/ijms161226218.

Si, D., Wang, Y., Zhou, Y.-H., Guo, Y., Wang, J., Zhou, H., Li, Z.-S., Fawcett, J.P., 2009. Mechanism of CYP2C9 inhibition by flavones and flavonols. Drug Metab. Dispos. 37, 629–634. https://doi.org/10.1124/dmd.108.023416.

Su, C.-C., Chiu, T.-L., 2016. Tanshinone IIA decreases the protein expression of EGFR, and IGFR blocking the PI3K/Akt/mTOR pathway in gastric carcinoma AGS cells both in vitro and in vivo. Oncol. Rep. 36, 1173–1179. https://doi.org/10.3892/or.2016.4857.

Takizawa, Y., Morota, T., Takeda, S., Aburada, M., 2003. Pharmacokinetics of (-)-epicatechin-3-O-gallate, an active component of Onpi-to, in rats. Biol. Pharm. Bull. 26, 608–612. https://doi.org/10.1248/bpb.26.608.

Taylor, D.K., Leppert, P.C., 2012. Treatment for Uterine Fibroids: Searching for Effective Drug Therapies. Drug Discov. Today. Ther. Strateg. 9, e41–e49. https://doi.org/10.1016/j.ddstr.2012.06.001.

Tiwari, A., Tiwari, V., Verma, N., Singh, A., Kumar, M., Saini, V., Sahoo, B.M., Kaushik, D., Verma, R., Sagadevan, S., 2022. Molecular docking studies on the phytoconstituents as therapeutic leads against SARS-CoV-2. Polimery 67 (7–8), 355–374. https://doi.org/10.14314/polimery.2022.7.8.

Tzeng, S.H., Ko, W.C., Ko, F.N., Teng, C.M., 1991. Inhibition of platelet aggregation by some flavonoids. Thromb. Res. 64, 91–100. https://doi.org/10.1016/0049-3848(91)90208-e.

Vafadar, A., Shabaninejad, Z., Movahedpour, A., Fallahi, F., Taghavipour, M., Ghasemi, Y., Akbari, M., Shafiee, A., Hajighadimi, S., Moradizarmehri, S., 2020. Quercetin and cancer : new insights into its therapeutic effects on ovarian cancer cells. Cell Biosci. 10, 1–17. https://doi.org/10.1186/s13578-020-00397-0.

Waffo-Téguo, P., Hawthorne, M.E., Cuendet, M., Mérillon, J.M., Kinghorn, A.D., Pezzuto, J.M., Mehta, R.G., 2001. Potential cancer-chemopreventive activities of wine stilbenoids and flavans extracted from grape (Vitis vinifera) cell cultures. Nutr. Cancer 40, 173–179. https://doi.org/10.1207/S15327914NC402_14.

Wang, N., He, J., Chang, A.K., Wang, Y., Xu, L., Chong, X., Lu, X., Sun, Y., Xia, X., Li, H., Zhang, B., Song, Y., Kato, A., Jones, G.W., 2015. (-)-epigallocatechin-3-gallate inhibits fibrillogenesis of chicken cystatin. J. Agric. Food Chem. 63, 1347–1351. https://doi.org/10.1021/jf505277e.

Wang, C.C., Xu, H., Man, G.C.W., Zhang, T., Chu, K.O., Chu, C.Y., Cheng, J.T.Y., Li, G., He, Y.X., Qin, L., Lau, T.S., Kwong, J., Chan, T.H., 2013. Prodrug of green tea epigallocatechin-3-gallate (Pro-EGCG) as a potent anti-angiogenesis agent for endometriosis in mice. Angiogenesis 16, 59–69. https://doi.org/10.1007/s10456-012-9299-4.

Wang, J., Xu, J., Wang, B., Shu, F.R., Chen, K., Mi, M.T., 2014. Equol promotes rat osteoblast proliferation and differentiation through activating estrogen receptor. Genet. Mol. Res. 13, 5055–5063. https://doi.org/10.4238/2014.July.4.21.

Wang, Z., Zhang, H., Zhou, J., Zhang, X., Chen, L., Chen, K., Huang, Z., 2016. Eriocitrin from lemon suppresses the proliferation of human hepatocellular carcinoma cells through inducing apoptosis and arresting cell cycle. Cancer Chemother. Pharmacol. 78, 1143–1150. https://doi.org/10.1007/s00280-016-3171-y.

Wu, K., Yuan, L.-H., Xia, W., 2005. Inhibitory effects of apigenin on the growth of gastric carcinoma SGC-7901 cells. World J. Gastroenterol. 11, 4461–4464. https://doi.org/10.3748/wjg.v11.i29.4461.

Xie, J., Liu, J., Liu, H., Liang, S., Lin, M., Gu, Y., Liu, T., Wang, D., Ge, H., Mo, S.-L., 2015. The antitumor effect of tanshinone IIA on anti-proliferation and decreasing VEGF/VEGFR2 expression on the human non-small cell lung cancer A549 cell line. Acta Pharm. Sin. B 5, 554–563. https://doi.org/10.1016/j.apsb.2015.07.008.

Xu, J., Wei, K., Zhang, G., Lei, L., Yang, D., Wang, W., Han, Q., Xia, Y., Bi, Y., Yang, M., Li, M., 2018. Ethnopharmacology, phytochemistry, and pharmacology of Chinese Salvia species: A review. J. Ethnopharmacol. 225, 18–30. https://doi.org/10.1016/j.jep.2018.06.029.

Xu, Y., Xie, Q., Wu, S., Yi, D., Yu, Y., Liu, S., Li, S., Li, Z., 2016. Myricetin induces apoptosis via endoplasmic reticulum stress and DNA double-strand breaks in

human ovarian cancer cells. Mol Med Rep 13, 2094–2100. https://doi.org/10.3892/mmr.2016.4763.
Yang, F., Song, L., Wang, H., Wang, J., Xu, Z., Xing, N., 2015. Combination of Quercetin and 2-Methoxyestradiol Enhances Inhibition of Human Prostate Cancer LNCaP and PC-3 Cells Xenograft Tumor Growth. PLoS One 10, e0128277.
Zhang, Z., Li, Y., Sheng, C., Yang, C., Chen, L., Sun, J., 2016. Tanshinone IIA inhibits apoptosis in the myocardium by inducing microRNA-152-3p expression and thereby downregulating PTEN. Am. J. Transl. Res. 8, 3124–3132.
Zhang, Y., Zhang, R., Ni, H., 2020. Eriodictyol exerts potent anticancer activity against A549 human lung cancer cell line by inducing mitochondrial-mediated apoptosis, G2/M cell cycle arrest and inhibition of m-TOR/PI3K/Akt signalling pathway. Arch. Med. Sci. 16, 446–452. https://doi.org/10.5114/aoms.2019.85152.